JACC: BASIC TO TRANSLATIONAL SCIENCE
VOL. 2, NO. 6, 2017
ISSN 2452-302X
https://doi.org/10.1016/j.jacbts.2017.08.002

PRECLINICAL RESEARCH

Transplantation of Allogeneic PW1^{pos}/Pax7^{neg} Interstitial Cells Enhance Endogenous Repair of Injured Porcine Skeletal Muscle

Fiona C. Lewis, BSc, PhD,[a] Beverley J. Cottle, BSc, PhD,[a] Victoria Shone, BSc, MSc, PhD,[a] Giovanna Marazzi, MD,[b] David Sassoon, PhD,[b] Cheyenne C.S. Tseng, MD,[c] Patricia Y.W. Dankers, PhD,[d] Steven A.J. Chamuleau, MD, PhD,[c] Bernardo Nadal-Ginard, MD, PhD,[a] Georgina M. Ellison-Hughes, BSc, PhD[a]

VISUAL ABSTRACT

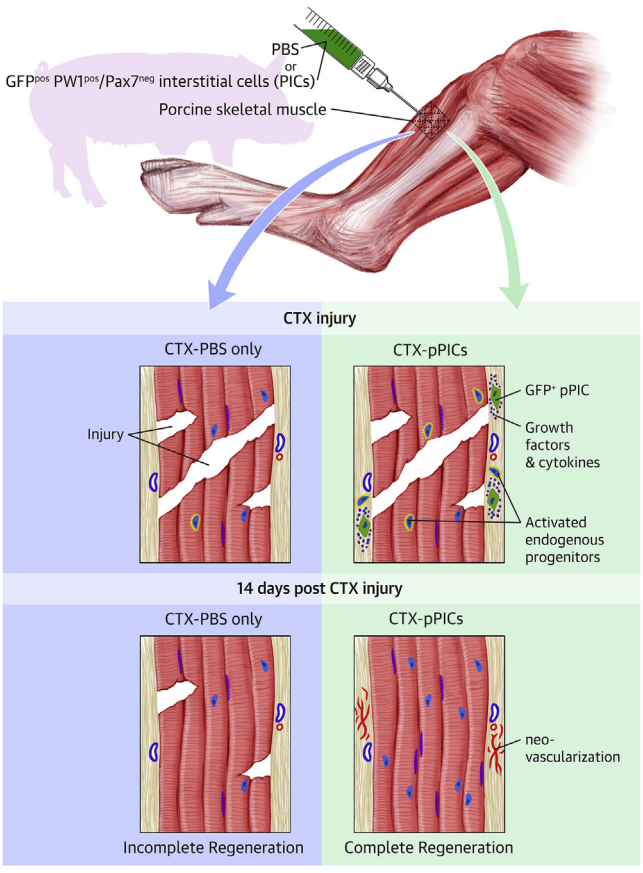

Lewis, F.C. et al. J Am Coll Cardiol Basic Trans Science. 2017;2(6):717–36.

HIGHLIGHTS

- **Allogeneic PICs express and secrete an array of pro-regenerative paracrine factors that stimulate a regenerative response in a preclinical muscle injury model applicable to humans.**
- **Paracrine factors secreted by allogeneic PICs stimulate endogenous progenitor cell activation and differentiation, leading to accelerated and improved myofiber regeneration and microvessel formation.**
- **Allogeneic PICs survive long enough to exert their action before being cleared by the host immune system. Therefore, the cells transplanted are allogeneic but the regeneration is completely autologous.**
- **Administration of HGF and IGF-1 improves skeletal muscle regeneration, but not to the same extent as PIC transplantation.**

ABBREVIATIONS AND ACRONYMS

BrdU = 5-bromo-2′-deoxyuridine

CM = pPIC conditioned medium

CSA = cross sectional area

CSC = cardiac stem cell

CTRL = control

CTX = cardiotoxin

FBS = fetal bovine serum

DAPI = 4′,6-diamidino-2-phenylindole

DMEM = Dulbecco's Modified Eagle's medium

GFPpPIC = GFP-positive porcine PW1^{pos}/Pax7^{neg} interstitial cell

GM = growth medium

HUVEC = human umbilical vein endothelial cell

HVG = hematoxylin and van Gieson

ICM = heat-inactivated conditioned medium

IV = intravenous

MHC = myosin heavy chain

MI = myocardial infarction

nMHC = neonatal myosin heavy chain

P = passage

PBMC = peripheral blood mononuclear cell

PBS = phosphate buffered saline

PIC = PW1^{pos}/Pax7^{neg} interstitial cell

pPIC = porcine PW1^{pos}/Pax7^{neg} interstitial cell

qRT-PCR = quantitative reverse transcription polymerase chain reaction

TA = tibialis anterior

UM = unconditioned medium

vWF = Von Willebrand factor

SUMMARY

Skeletal muscle-derived PW1^{pos}/Pax7^{neg} interstitial cells (PICs) express and secrete a multitude of proregenerative growth factors and cytokines. Utilizing a porcine preclinical skeletal muscle injury model, delivery of allogeneic porcine PICs (pPICs) significantly improved and accelerated myofiber regeneration and neocapillarization, compared with saline vehicle control-treated muscles. Allogeneic pPICs did not contribute to new myofibers or capillaries and were eliminated by the host immune system. In conclusion, allogeneic pPIC transplantation stimulated the endogenous stem cell pool to bring about enhanced autologous skeletal muscle repair and regeneration. This allogeneic cell approach is considered a cost-effective, easy to apply, and readily available regenerative therapeutic strategy. (J Am Coll Cardiol Basic Trans Science 2017;2:717–36)

Skeletal muscle is a dynamic, highly plastic tissue that is capable of undergoing repair and regeneration in healthy individuals (1). However, this regenerative capacity can become impaired in muscle diseases, such as muscular dystrophy, and as a result of disuse and ageing (2,3). This leads to decreased proliferation, delayed fusion, and reduced differentiation of muscle progenitors, as well as a gradual replacement of muscle fibers by fat and fibrosis with poor vascularization (4,5). The mechanisms that underpin impaired skeletal muscle regeneration are still unclear; however, recent findings suggest that the microenvironment and/or systemic factors (6,7) affect the response of various endogenous skeletal muscle progenitor cells to repair and regenerate after injury (8). This has led us to focus upon therapeutic strategies that target resident muscle progenitors and stimulate endogenous repair mechanisms.

Autologous stem cell approaches are attractive from a theoretical and biological standpoint; however, for skeletal muscle where the muscle satellite cells cannot be effectively propagated to large numbers in vitro, and like other tissue-specific stem/progenitor cells, such as cardiac, are affected by age and disease, they are impractical. Moreover, administration of cells can induce therapeutic responses by indirect means, such as secretion of growth factors and interaction with endogenous repair processes, represented by the resident stem/progenitor cells (9,10). This has been termed the paracrine effect. Therefore, there seems to be little advantage in the use of autologous cells because a similar, and perhaps enhanced, effect can be obtained by the administration of a cell type isolated from allogeneic sources, which could be made readily available at reduced costs (11). We have previously shown that intracoronary injection of allogeneic porcine cardiac stem cells (CSCs) after myocardial infarction (MI) activates the endogenous, resident CSCs through a paracrine mechanism, resulting in improved myocardial cell survival, function, remodeling, and regeneration (12).

Skeletal muscle satellite cells, although capable of muscle fiber regeneration, have a limited migration capacity with an inability to cross the endothelial wall (13). Moreover, cultured satellite cells ex vivo have decreased stemness, proliferation, and myofiber differentiation, which has subsequently hampered their

From the [a]School of Basic & Medical Biosciences, Centre of Human & Aerospace Physiological Sciences & Centre for Stem Cells and Regenerative Medicine, Faculty of Life Sciences & Medicine, King's College London, Guy's Campus, London, United Kingdom; [b]Stem Cells and Regenerative Medicine UMRS 1166, Institute of Cardiometabolism and Nutrition, Université de Pierre et Marie Curie, Sorbonne Universités, Paris, France; [c]Department of Cardiology, Division of Heart and Lungs, University Medical Center Utrecht, Utrecht, the Netherlands; and the [d]Supramolecular Biomaterials for Translational Biomedical Science, Department of Biomedical Engineering, Eindhoven University of Technology, Eindhoven, the Netherlands. This work was supported by the European Research Council, European Community 7th Framework project ENDOSTEM (contract number FP7-Health-2009-ENDOSTEM 241440 Activation of vasculature-associated stem cells and muscle stem cells for the repair and maintenance of muscle tissue). The authors have reported that they have no relationships relevant to the contents of this paper to disclose. Drs. Nadal-Ginard and Ellison-Hughes contributed equally to this work. All authors attest they are in compliance with human studies committees and animal welfare regulations of the authors' institutions and Food and Drug Administration guidelines, including patient consent where appropriate. For more information, visit the *JACC: Basic to Translational Science* author instructions page.

Manuscript received March 17, 2017; revised manuscript received August 16, 2017, accepted August 16, 2017.

translation (14). In recent years, skeletal muscle has been shown to harbor other stem/progenitor cells, such as the $PW1^{pos}/Pax7^{neg}$ interstitial cells (PICs), which are bipotent, giving rise to new skeletal muscle fibers and vasculature-associated cell types in vitro and in vivo (15,16). Unlike the satellite cells, we have shown that porcine PICs (pPICs) can be successfully isolated and propagated in vitro up to passage 40 (P40) while maintaining a stable phenotype/genotype (16). Therefore PICs represent an attractive and alternative cell source for regenerative therapies.

The pig represents an excellent biological model for human biomedical preclinical research due to its anatomic, physiological, pathological, and genomic similarities to humans (17). In terms of porcine skeletal muscle biology, considerable correlation between contractile, metabolic, and morphological features to human skeletal muscle exist (18–20). Although small animal models are a valuable resource, they do not always accurately reflect the clinical manifestation, with many cell therapies that have been shown to be highly effective in small animal models (21,22) yielding only modest therapeutic value in human clinical trials (23,24). Combined with the 3 orders of magnitude difference in mass between rodent models and humans, there is an obvious need to test cell therapies in more illustrative animal models. Developing a porcine preclinical model for skeletal muscle regeneration can provide a useful link between the widely used rodent models and humans so that an improved prediction of therapeutic efficacy of therapies can be achieved and successfully translated to patients. Moreover, unlike other organs, skeletal muscle is an efficient regenerative tissue yielding adequate resident progenitor cells, which give rise to new myofibers and vasculature following injury. Altogether, this makes the porcine skeletal muscle an appropriate model system to test proof-of-concept regenerative therapeutic approaches, such as the allogeneic cell approach, described here for the first time to our knowledge. Allogeneic stem cell therapy is conceptually and practically different from any presently in clinical use and could be applied in the repair and regeneration of other tissues, such as the heart.

Here, we tested the therapeutic reparative effect of delivering allogeneic pPICs to the injured pig skeletal muscle. We hypothesized that allogeneic pPICs transplanted following skeletal muscle injury would supply regenerative bioactive factors capable of activating the endogenous stem/progenitor cells, enhancing and accelerating the regeneration of damaged skeletal muscle tissue. It was also hypothesized that the allogeneic pPICs survive long enough in the allogeneic host to produce their paracrine effect activating the endogenous target cells before being eliminated by the host immune system. Therefore, the cells transplanted are allogeneic, but the regeneration is completely autologous.

METHODS

STUDY DESIGN, SKELETAL MUSCLE INJURY, AND INTRAMUSCULAR pPIC ADMINISTRATION. Animals were immune competent, 2-month-old (juvenile), female, large Dalland Landrace pigs (32 ± 5 kg). All animal procedures were performed in accordance with the EU Directive guidelines and regulations for animal experimentation by appropriately qualified staff and approved by the institutional animal welfare and ethical review board DEC Utrecht, the Netherlands. Pigs were sedated with 4 mg/kg thiopental sodium, and anesthesia was maintained with midazolam (0.5 mg/kg/h) via an intravenous (IV) catheter placed in a peripheral ear vein before intubation. The animals were subsequently moved to the surgery room and secured to the surgical table with limb bindings. The lower hind limb was shaved and disinfected using iodine before surgery.

The first phase of the in vivo study used 6 pigs. In order to assess 2 different injury models, either an open freeze/crush (n = 3) or cardiotoxin (CTX) injury (n = 3) of the tibialis anterior (TA) muscle was subsequently performed. Briefly, a 5-cm longitudinal incision of the skin and underlying fascia was made along the anterior aspect of the distal limb. The skin and fascia were retracted, the TA muscle located, nonabsorbable Prolene sutures (Ethicon, Somerville, New Jersey) were used to mark the injury site (1 cm × 1 cm^2), and the injury was induced. In the case of freeze/crush injury, the muscle was crushed with forceps (Fine Science Tools, Foster City, California), pre-cooled in liquid nitrogen. This procedure was repeated 7 times for 5 s each, in direct continuity with the respective distal crush in the defined area. In the case of CTX injury induction, a 10 μmol/l CTX solution, *Naja mossambica mossambica* (Sigma-Aldrich, St. Louis, Missouri), was filtered and brought to room temperature before injection. The CTX was dispersed in a series of 5 intramuscular injections using a 25-ga needle to deliver a total volume of 500 μl to the predefined area. The contralateral leg served as a sham control (CTRL) and was treated identically; however, no injury was applied in the case of freeze/crush, or phosphate buffered saline (PBS) alone was injected in animals receiving the CTX injury. The injury area was identified through marking with sutures. After injury induction, the superficial skin was sutured; animals

were allowed to recover and then sacrificed by anesthetic overdose at either 14 or 21 days post-injury.

In the second phase of the in vivo study, 10 pigs were randomly assigned to receive either saline vehicle (PBS) or allogeneic GFP^{pos} pPICs, 15 min post-CTX injury. GFP^{pos} pPICs were propagated and cryostored between P3 and P12. Before transplantation, GFP^{pos} pPICs were pre-mixed, brought into suspension, centrifuged, washed twice with PBS, and then counted. A total of 20×10^6 GFP^{pos} pPICs were resuspended in 500 μl of PBS and injected intramuscularly into the injured TA through a 25-ga needle ($n = 5$). Control animals were treated identically; however, 500 μl of PBS alone was injected ($n = 5$). Both treatments were distributed across 5 injection sites to the injury site. The contralateral control leg of each animal served as a sham CTRL and received no injury, only PBS, using the same protocol.

In separate pigs, local delivery of human recombinant insulin-like growth factor (IGF)-1 (8 μg) and hepatocyte growth factor (HGF) (2 μg) (Peprotech, Rocky Hill, New Jersey) was achieved by diluting both growth factors in a total volume of 500 μl of PBS before being dispersed in a series of 5 intramuscular injections using a 25-ga needle to deliver the total volume to the pre-defined injured area ($n = 5$). In the case of ureido-pyrimidinone (UPy)+IGF-1/HGF treatment, the UPy hydrogelators were synthesized by SyMO-Chem BV (Eindhoven, the Netherlands), as described previously (25). To prepare the hydrogel, polymer solutions were dissolved at 10% by weight in PBS by stirring at 70°C for 1 h and were subsequently cooled to room temperature. To liquefy the polymer solution, the pH was increased to pH 8.5 by adding 2-μl aliquots of a 0.1 mol/l NaOH stock solution. The hydrogel was then sterilized with ultraviolet light for 1 h, and human recombinant IGF-1 and HGF were added before use, yielding a final concentration of 8 μg and 2 μg, respectively. A total volume of 500 μl of UPy hydrogel+IGF-1/HGF was administered as per the method described in the preceding text ($n = 5$).

In order to track newly formed cells post-injury, we used the thymidine analogue, 5-bromo-2′-deoxyuridine (BrdU). In order to deliver BrdU to the animals over the course of the regeneration period, we used an IV delivery system. This involved making a channel through the pig's neck musculature and feeding an IV line through, which was subsequently connected to the jugular vein. This enabled us to access a cannula situated on the dorsal aspect of the pig's neck, which was directly linked to circulation system. This method allowed daily administration of BrdU at a dose of 10 mg/kg/day without the need to sedate the animals. Animals were sacrificed by anesthetic overdose at 14 days post-injury.

CELL CULTURE. Porcine PICs were isolated and maintained as previously described (16) in growth medium (GM); Dulbecco's Modified Eagle's medium/Ham's F12 (DMEM/F12; Sigma-Aldrich): Neurobasal A (Thermo Fisher Scientific, Waltham, Massachusetts) medium (1:1) containing 10% embryonic stem cell qualified fetal bovine serum (ESQ-FBS) (Invitrogen, Carlsbad, California), B-27 and N-2 supplements (Thermo Fisher Scientific), leukemia inhibitory factor (LIF) (10 ng/ml; Millipore, Billerica, Massachusetts), basic fibroblast growth factor (bFGF) (10 ng/ml; Peprotech), epidermal growth factor (EGF) (20 ng/ml; Peprotech), insulin-transferrin-selenium 2% GlutaMAX (Thermo Fisher Scientific), 1% penicillin-streptomycin (Thermo Fisher Scientific), and 0.1% gentamicin (10 mg/ml; Thermo Fisher Scientific). Myogenic differentiation was induced by replacing GM with DMEM/F12, 2% horse serum 2% GlutaMAX (Thermo Fisher Scientific) for either 24 h or 5 days. Human myoblasts were isolated and maintained as previously described (26). Human umbilical vein endothelial cells (HUVECs) (Lonza, Basel, Switzerland) were cultured in endothelial cell GM supplemented with 2% FBS and growth factors (Lonza).

GFP TRANSDUCTION OF pPICs. To generate green fluorescent protein (GFP) lentivirus, HEK293T cells were cultured overnight in dishes pre-coated with 0.1 mg/ml collagen solution (Sigma-Aldrich) in DMEM, 10% fetal calf serum (FCS), 2% GlutaMAX, and 1% penicillin-streptomycin until 70% confluent. The following day, a mix of 6.5 μg of pCMV Δ8.9 packaging plasmid, 3.5 μg VSV-g envelope plasmid, and 10 μg GFP expression construct were diluted in 500 μl of OptiMEM-1 (Thermo Fisher Scientific) without FCS or antibiotics. A second mixture, containing 30 μl of Lipofectamine 2000 (Thermo Fisher Scientific) in 500 μl of OptiMEM-1 without FCS or antibiotics was added to the plasmid mix solution and incubated at room temperature for 20 min, inverting the tube every 5 min. The plasmid/Lipofectamine mixture was added dropwise to the HEK293T cells and incubated at 37°C for 4 h. After 4 h, an equal volume of OptiMEM-1 with the addition of 10% FCS and 1% penicillin-streptomycin was added. The supernatant was collected 48 h post-transfection and filtered with a 0.45-μm filter. The viral supernatant was subsequently concentrated using a Lenti-X Concentrator kit (Clontech, Mountain View, California) according to the manufacturer's specification, and the viral titer was

measured using GoStix (Clontech). The pseudovirus was subsequently used for transduction or stored at −80°C. Target pPICs at P2 were transduced by adding 30 μl/ml pseudovirus in DMEM, 10% FCS containing 12 μg/ml polybrene (Sigma-Aldrich). After 24 h, the medium was changed to DMEM with the addition of serum and antibiotics. The infected target cells were further cultured and analyzed at 24 h post-transduction for GFP expression, using fluorescent microscopy and flow cytometry. Porcine PICs transduced with the GFP reporter gene were propagated for allogeneic transplantation experiments in pPIC GM.

FLOW CYTOMETRY. Flow cytometry was performed as previously described (16). Immunophenotyping was performed using the following antibodies; PW1 (antibody kindly gifted by D. Sassoon), CD34 (Thermo Fisher Scientific), CD45 (AbD Serotec, Puchheim, Germany), and Pax7 (Developmental Studies Hybridoma Bank, Iowa City, Iowa). Isotype controls were used to define the specific gates and analysis was performed using a FACSCanto II with FACSDiva software (BD Biosciences, San Jose, California).

TISSUE PROCESSING AND HISTOLOGY. Whole TA muscles were excised, washed in PBS, weighed, and then fixed in 10% formalin (Sigma-Aldrich) with gentle agitation for 4 days. Muscles were processed for paraffin embedding using a Leica TP1020 tissue processor (Leica Biosystems, Buffalo Grove, Illinois) as previously described (16). To measure myofiber diameter and identify fibrosis, muscle sections were stained with hematoxylin and van Gieson (HVG) (Sigma-Aldrich), respectively, according to standard procedures (27). Cross-sectional area (CSA) of connective tissue was determined from 5 fields of view at ×20 magnification per muscle using a light microscope (Olympus, Tokyo, Japan) and ImageJ2 software (NIH, Bethesda, Maryland). To determine the mean myofiber diameters, measurements were performed on transverse sections with 100 myofibers analyzed per section.

IMMUNOHISTOCHEMISTRY/IMMUNOCYTOCHEMISTRY. To identify regenerating muscle fibers, muscle sections were stained with anti-human neonatal myosin heavy chain (nMHC) (Developmental Studies Hybridoma Bank). Sections were also stained with anti-laminin (Abcam, Cambridge, United Kingdom) to identify the basal lamina of individual fibers and centralized nuclei identified through 4′,6-diamidino-2-phenylindole (DAPI) (Sigma-Aldrich) staining. All newly formed cells were identified by anti-BrdU (Roche, Basel, Switzerland) staining. The number of centralized nuclei was determined by counting 5 fields/section at ×20 magnification. A total of 5 slides/animal were assessed capillary density was evaluated by staining with an antibody against von Willebrand factor (vWF) (Dako, Glostrup, Denmark). The number of capillaries (defined as 1 or 2 endothelial cells spanning the vWF-positive vessel circumference) was determined by counting 5 fields/section at ×20 magnification. A total of 5 slides/animal was assessed, and the amount of capillaries was expressed per number of myofibers. Double staining for BrdU/vWF was performed to identify newly formed capillaries and counterstained with DAPI to detect nuclei. Tracking of donor GFP^{pos} cells was achieved by staining with anti-GFP (Rockland, Limerick, Pennsylvania). GFP^{pos} cells were quantified by counting 5 fields/section at ×20 magnification. A total of 5 slides/animal were assessed, and the number of GFP^{pos} cells quantified. To identify whether transplanted cells retained their PIC phenotype in vivo, tissue sections were stained for PW1 (antibody kindly gifted by D. Sassoon) and Pax7 (Developmental Studies Hybridoma Bank). Bipotent myogenic differentiation was assessed by staining for myosin heavy chain (MHC) (Developmental Studies Hybridoma Bank) and smooth muscle actin (Sigma-Aldrich) as previously described (16). Immune cells were identified by staining with anti-CD8a (Abcam), anti-Granzyme B (Abcam) or anti-IBA-1 (Wako, Osaka, Japan). Immune cells were quantified by imaging 5 fields/section at ×20 magnification. All secondary antibodies were purchased from Thermo Fisher Scientific. In all cases, an ApoTome fluorescent microscope (Carl Zeiss, Oberkochen, Germany) was used to obtain images for quantification and representative images were acquired using a confocal microscope (Nikon A1R, Nikon, Tokyo, Japan). Analysis was subsequently performed using ImageJ software.

GENE EXPRESSION PROFILING. To identify growth factors and cytokines expressed by undifferentiated and early myogenic differentiated pPICs, gene array analyses were performed (n = 3/group). RNA was extracted from pPICs that were either maintained in an undifferentiated condition in standard GM or placed in a myogenic permissive environment (DMEM/F12, 2% horse serum) for 24 h. Total RNA was isolated using the Qiagen RNeasy Mini Kit and reverse transcribed using the RT2 first strand kit (Qiagen, Hilden, Germany) according to the manufacturer's recommendations for the RT2 Profiler PCR Array. Quantitative reverse transcription polymerase chain reaction (qRT-PCR) was then performed using RT2 SYBR Green (Qiagen) and the RT2 Profiler PCR Array

(Qiagen), which was custom designed for the identification of porcine growth factors and cytokines of interest. Briefly, samples were denatured for 10 min at 95°C, cycled 40 times at 95°C for 15 s, followed by 40 cycles at the annealing temperature of 60°C for 1 min on a MyIQ thermocycler (Bio-Rad, Hercules, California). All reactions were carried out in triplicate; data were normalized to 5 housekeeping genes (*ACTB*, *B2M*, *GAPDH*, *HPRT1*, *RPL13A*) and analyzed using Bio-Rad IQ software (version 3.1).

WESTERN BLOTTING. Immunoblots were carried out using protein lysates obtained from undifferentiated pPICs and pPICs that had undergone early myogenic differentiation (n = 3/group). Approximately, 50 μg of protein were separated on gradient (10% to 15%) SDS-polyacrylamide gels. After electrophoresis, proteins were transferred onto nitrocellulose membranes and blocked with 5% milk, then incubated with antibodies against IGF-1 (Santa Cruz Biotechnology, Dallas, Texas), HGF (Santa Cruz Biotechnology), transforming growth factor (TGF)-β1 (Santa Cruz Biotechnology), neuregulin (NRG)-1 (Santa Cruz Biotechnology) at dilutions suggested by the manufacturers. GAPDH (Millipore) was used as a loading control. Proteins were detected by chemiluminescence using horseradish peroxidase–conjugated secondary antibodies (Santa Cruz Biotechnology) and visualized using ECL Plus Western Blotting Detection Reagents (Amersham, Little Chalfont, United Kingdom) and a Chemidoc imaging system (Bio-Rad).

BRDU PROLIFERATION ASSAY IN VITRO. pPICs and human myoblasts were plated in 24-well plates at a density of 5×10^3 per well and were serum starved for 6 h in 0% serum DMEM/F12 medium. To investigate the effect of pPIC conditioned media on proliferation, wells were either supplemented with standard GM, unconditioned medium (UM), pPIC conditioned medium (CM), or heat-inactivated conditioned medium (ICM). Each well was supplemented with BrdU (1 μg/ml) every 8 h, fixed in 4% paraformaldehyde after 24 h, and BrdU incorporation was then assessed using the BrdU detection kit (Roche) (n = 3/condition).

In order to investigate the effect of growth factors on pPIC proliferation, wells were serum starved for 6 h and then switched to basal media (control), or supplemented with IGF-1 (100 ng/ml; Peprotech), HGF (100 ng/ml; Peprotech), NRG-1 (100 ng/ml; R&D Systems, Minneapolis, Minnesota), or TGF-β1 (5 ng/ml; Peprotech). Each well was supplemented with BrdU (1 μg/ml) every 8 h, fixed after 24 h, and BrdU incorporation was assessed using the BrdU detection kit (Roche) (n = 3/growth factor). Nuclei were counterstained with DAPI. Cells were evaluated using an ApoTome fluorescent microscope (Carl Zeiss). The percentage of $BrdU^{pos}$ cells relative to the total number of cells was determined by counting 5 random fields at ×20 magnification for each dish, and then expressed as fold change over unsupplemented control.

MYOGENIC DIFFERENTIATION ASSAY IN VITRO. To assess the effect of different growth factors in the induction of myogenic differentiation in vitro, 1×10^4 pPICs were plated in 24-well plates on gelatin-coated coverslips in basal media (control). Individual growth factors (concentrations stated earlier in the text) were supplemented (n = 3 wells/growth factor). Three wells acted as controls, with no growth factors added to the medium. Cells were fixed in 4% paraformaldehyde after 5 days, and myogenic differentiation was quantified by staining for MHC (Developmental Studies Hybridoma Bank). Nuclei were counterstained with DAPI. Cells were evaluated using an ApoTome fluorescent microscope (Carl Zeiss), 5 random fields at ×20 magnification were quantified for each well, and the fusion index was calculated by counting the number of nuclei inside myotubes per total nuclei.

MATRIGEL ANGIOGENESIS ASSAY. To study angiogenesis, 150 μl of Matrigel substrate (Corning, Corning, New York) diluted with DMEM (1:10) was pipetted into each well of a 24-well plate and allowed to solidify for 1 h at 37°C. Thereafter, 2×10^4 HUVECs were seeded into each well in either endothelial GM (see details earlier in the text), UM (serum-free), CM, or ICM. Cells were imaged at 24 h using a light microscope (Olympus). Five fields of view at ×20 magnification were imaged for each condition. Parameters of angiogenesis (capillary area, number of tubes per field of view, tube length, and branching points) were analyzed using Wimasis image analysis software (WimTube Release 4.0, Onimagin Technologies, Córdoba, Spain).

CYTOTOXICITY ASSAY IN VITRO. Peripheral blood mononuclear cells (PBMCs) were isolated from pig whole blood using density gradient centrifugation with Histopaque (Sigma-Aldrich). Briefly, whole blood was diluted at the ratio of 1:1 with PBS and carefully layered over 6 ml of Histopaque solution. Tubes were centrifuged at 400 × *g* for 30 min at room temperature. PBMCs were then carefully collected from the buffy coat layer, washed twice with PBS, and frozen at −80°C until ready to use. PBMCs were resuscitated and cultured for 3 days in RPMI 1640 GlutaMAX medium (Thermo Fisher Scientific), 10% FBS, and 1% penicillin-streptomycin (Thermo Fisher Scientific). PBMCs were either maintained in medium

alone or activated with phytohemagglutinin (PHA) (Sigma-Aldrich) (5 μg/ml) for 3 days. PICs (P6) were plated at 1×10^5 per well in a 24-well plate, 1 day before co-culture. PBMCs were harvested and co-cultured with PICs in RPMI medium as follows; no PBMCS, 1:10, 1:20, and 1:40. After 4 h of co-culture, PBMCs were discarded; PICs were harvested and subsequently labelled with anti-CD45 antibody/Annexin V-PE Apoptosis Detection Kit I (BD Biosciences) and analyzed by flow cytometry using a FACSCanto II and FACS DIVA V8.0.1 software (BD Biosciences).

STATISTICAL ANALYSIS. Data are reported as mean ± SD. Significance between 2 groups was determined by paired samples Student's *t*-test and in multiple comparisons by analysis of variance. Holm-Šídák method was used to locate the differences. A probability of <5% ($p < 0.05$) was considered to be statistically significant. Data were analyzed using SPSS Statistics version 22 software (IBM, Armonk, New York).

RESULTS

CTX-INDUCED INJURY IS A REPRODUCIBLE MODEL OF PORCINE SKELETAL MUSCLE DAMAGE. In order to determine a robust model to investigate allogeneic pPIC regenerative therapy in vivo, 2 different models of porcine skeletal muscle damage were first evaluated. Freeze/crush and CTX injuries were assessed because they have been extensively used to model skeletal muscle damage in small animals (28). The freeze/crush injury is a segmental model of trauma, selectively affecting muscle fibers and interstitial tissue without disrupting the main innervation of the tissue. The CTX injury, induced using a series of CTX injections, is a diffuse injury model. All animals recovered from the surgical procedure without complications and were fully ambulatory within a few hours after surgery with only minor swelling observed at the surgical site. Histological assessment of explanted muscle revealed that the freeze/crush injury, as expected, was restricted to the superficial layer of muscle adjacent to a deep uninjured region (Supplemental Figure S1). CTX-injured muscles showed a diffuse pattern of damage throughout the tissue (Supplemental Figure S1). Both injuries resulted in significantly decreased muscle fiber CSA (CTX-injured 53 ± 7% per total area ($p < 0.0001$); freeze/crush-injured 66 ± 7% per total area ($p = 0.0015$), compared with uninjured contralateral control muscle (83 ± 4% per total area) (Supplemental Figure S1). Moreover, CTX-injured muscle exhibited a significant ($p < 0.018$) reduction in muscle fiber CSA, compared with freeze/crush-injured muscle (Supplemental Figure S1), showing that CTX injury damaged a greater number of myofibers. There was also a significant ($p < 0.01$) increase in the abundance of connective tissue in both injury models (Supplemental Figure S1). Both injuries resulted in an overall reduction in muscle fiber diameter, with CTX injury showing the greatest reduction (37.9 ± 8.5 μm), which was statistically significant ($p < 0.0001$), compared with uninjured control (63.3 ± 15.7 μm) (Supplemental Figure S1).

A decreased myofiber diameter implies the occurrence of small, newly formed, regenerating myofibers. Therefore, centralized nuclei, a marker of newly regenerated fibers, were evident in both injuries however they were more prevalent in the freeze/crush-injured muscle (27.27 ± 11.34 per 100 myofibers; $p < 0.0001$), compared with CTX-injured muscle (10.8 ± 6.0 per 100 myofibers) and uninjured CTRL (Supplemental Figure S1), suggesting that freeze/crush-injured muscles were more advanced in the regeneration process at 14 days post-injury, compared with CTX-injured muscles. Immunohistochemical staining of injured muscle was performed to determine the extent of regeneration with respect to early myosin isoforms. nMHC staining was observed in both larger fibers and small angular myofibers of CTX- and freeze/crush-injured muscle at 14 days post-injury (Supplemental Figure S1), and in the freeze/crush injury, nMHC expressing myofibers were restricted to the uppermost superficial layer of the muscle. The CTX-injured muscles showed a diffuse pattern of nMHC expression, and $nMHC^{pos}$ myofibers were more prevalent in CTX-injured muscle (37.2 ± 5.7%) compared with freeze/crush-injured muscle (25.6 ± 5.3%). $nMHC^{pos}$ fibers were also smaller in CTX-injured muscle (21.7 ± 4.9 μm) compared with those identified in the freeze/crush-injured muscle (24.8 ± 5.3 μm), supporting our observation that freeze/crush injury regeneration is more advanced at 14 days compared with CTX injury, which induces widespread injury with incomplete regeneration at 14 days (Supplemental Figure S1).

These results confirmed that CTX injury is a reproducible and diffuse injury model for testing skeletal muscle regeneration in the pig. However, in order to confirm whether 14 days was an appropriate time point for studying porcine skeletal muscle regeneration, a subset of animals were also sacrificed 21 days post-CTX injury. Immunohistochemical staining of muscle cross sections revealed that at 21 days, while there was a significant difference between the muscle fiber CSA (75 ± 3% muscle fiber per total area), compared with uninjured control (82 ± 3% muscle fiber per total area) ($p = 0.0027$), this was largely reduced compared to 14 days post-injury (Supplemental Figure S2). These

findings suggest that 21 days after CTX injury the muscle has undergone almost complete regeneration. Therefore, to measure whether allogeneic pPIC transplantation could enhance the regeneration of skeletal muscle, CTX was selected as the injury model with sacrifice of the pigs at 14 days post-injury.

TRANSPLANTATION OF ALLOGENEIC GFP^{pos} pPICs IMPROVES SKELETAL MUSCLE ARCHITECTURE AND ACCELERATES MYOFIBER REGENERATION. pPICs, which have previously been phenotyped and propagated over long term culture maintaining phenotypic and genomic stability (16), were transduced with a lentiviral vector encoding a GFP reporter. A total of 87.2% of pPICs were GFP-positive (GFPpPICs) as determined by flow cytometry (Supplemental Figure S3). GFPpPICs were propagated over 9 passages (P3 to P12) to generate the required number of cells for transplantation (20×10^6 per animal). GFPpPICs maintained a PIC phenotype after GFP transduction, which was stable up to P12, remaining positive for PW1 and CD34, and negative for CD45 and Pax7 (Supplemental Figure S3). Furthermore, GFPpPICs at P12 were comparable in their gene expression profile and bipotent differentiation potential to unlabeled pPICs (Supplemental Figure S3).

Initial histological observations indicated that pPIC-treated muscle had significantly improved muscle architecture and increased BrdU^{pos} centralized myonuclei, indicative of undergoing accelerated regeneration, compared with CTX-PBS-treated muscle (**Figures 1A and 1B**). There was a significant ($p < 0.001$) increase in muscle fiber CSA in pPIC-treated muscle (78 ± 5% per total area), compared with CTX-PBS (62 ± 2% per total area) (**Figure 1C**), and the ratio of muscle fiber to connective tissue CSA of pPIC-treated muscle (78% : 22 ± 5% per total area) at 14 days was closer to uninjured contralateral control muscle (87% : 13 ± 3% per total area) (**Figure 1C**).

Immunohistochemistry revealed a marked increase ($p = 0.0012$) in the number of centralized, BrdU^{pos} myofiber nuclei, which indicates newly regenerated fibers, in pPIC-treated muscles (15 ± 3%/total myofibers), compared with CTX-PBS-treated muscles (2 ± 1%/total myofibers) (**Figures 1B and 1D**). The uninjured contralateral control muscle had a very low number of BrdU^{pos} nuclei and centralized nuclei, indicating the low turnover of skeletal myofibers in uninjured, resting muscle (0.04 ± 0.08%) (**Figures 1B and 1D**). The diameter of the BrdU^{pos} regenerating myofibers in pPIC-treated muscles were found to be significantly larger ($p < 0.0001$) (41.4 ± 10 μm) than those of CTX-PBS-treated muscles (23.8 ± 7.3 μm) 14 days post-injury (**Figure 1E**). Taken together, these findings support an improved and accelerated regeneration of injured skeletal muscle, following transplantation of allogeneic pPICs.

ALLOGENEIC pPICs STIMULATE NEOANGIOGENESIS WHEN TRANSPLANTED INTO INJURED PORCINE SKELETAL MUSCLE. Immunohistochemical staining revealed a significant ($p < 0.0001$) increase in capillary density with CTX-pPIC treatment, compared with CTX-PBS and uninjured muscle (**Figures 2A and 2B**). Moreover, the presence of BrdU^{pos}/vWF^{pos} capillaries in the pPIC-treated muscle confirmed their formation post-injury and pPIC transplantation (**Figure 2C**). Quantification revealed a significant ($p < 0.0001$) increase in the number of BrdU^{pos}/vWF^{pos} capillaries in pPIC-treated skeletal muscle (94 ± 3% per total capillaries), compared with CTX-PBS-treated (56 ± 3% per total capillaries) skeletal muscle (**Figure 2D**). These findings show that allogeneic pPIC therapy stimulated angiogenesis in the injured skeletal muscle.

ALLOGENEIC pPIC TRANSPLANTATION ACTIVATES ENDOGENOUS PICs. To determine whether GFPpPIC transplantation had stimulated the activation of endogenous progenitor cells, sections were stained for PW1, Pax7, and GFP. We found a significant ($p = 0.0145$) increase in the number of endogenous PW1^{pos}/Pax7^{neg}/GFP^{neg} PICs in skeletal muscle that had been treated with allogeneic GFPpPICs (7.9 ± 1.9%/total nuclei), compared with CTX-PBS-treated CTRL (4.6 ± 0.5%/total nuclei) (**Figures 3A and 3B**). We also quantified the number of PW1^{pos}/Pax7^{pos}/GFP^{neg} satellite cells and found that pPIC treatment did not significantly alter the number of satellite cells (2.6 ± 0.4%/total nuclei), compared with CTX-PBS treatment (2.4 ± 0.5%/total nuclei) (**Figures 3C and 3D**). These data show that at 14 days post-injury, allogeneic pPIC transplantation had a stimulatory effect on the endogenous pPICs population, resulting in an increase in their number.

ALLOGENEIC GFP^{pos} pPICs ARE CLEARED BY THE HOST'S IMMUNE SYSTEM. To determine whether allogeneic GFPpPICs had persisted in the skeletal muscle and directly contributed to the regeneration, or as expected, had been cleared by the host's immune system, skeletal muscle cross sections were costained for GFP and laminin. Only a few GFPpPICs (1 GFP^{pos} nuclei/1,560 counted) persisted within the skeletal muscle 14 days post-injury (**Figures 4A and 4B**). Moreover, we found that the very few donor GFPpPICs that had remained had taken up residence within the interstitial spaces and maintained expression of

FIGURE 1 Transplantation of GFP^{pos} Allogeneic pPICs Accelerates Skeletal Muscle Regeneration

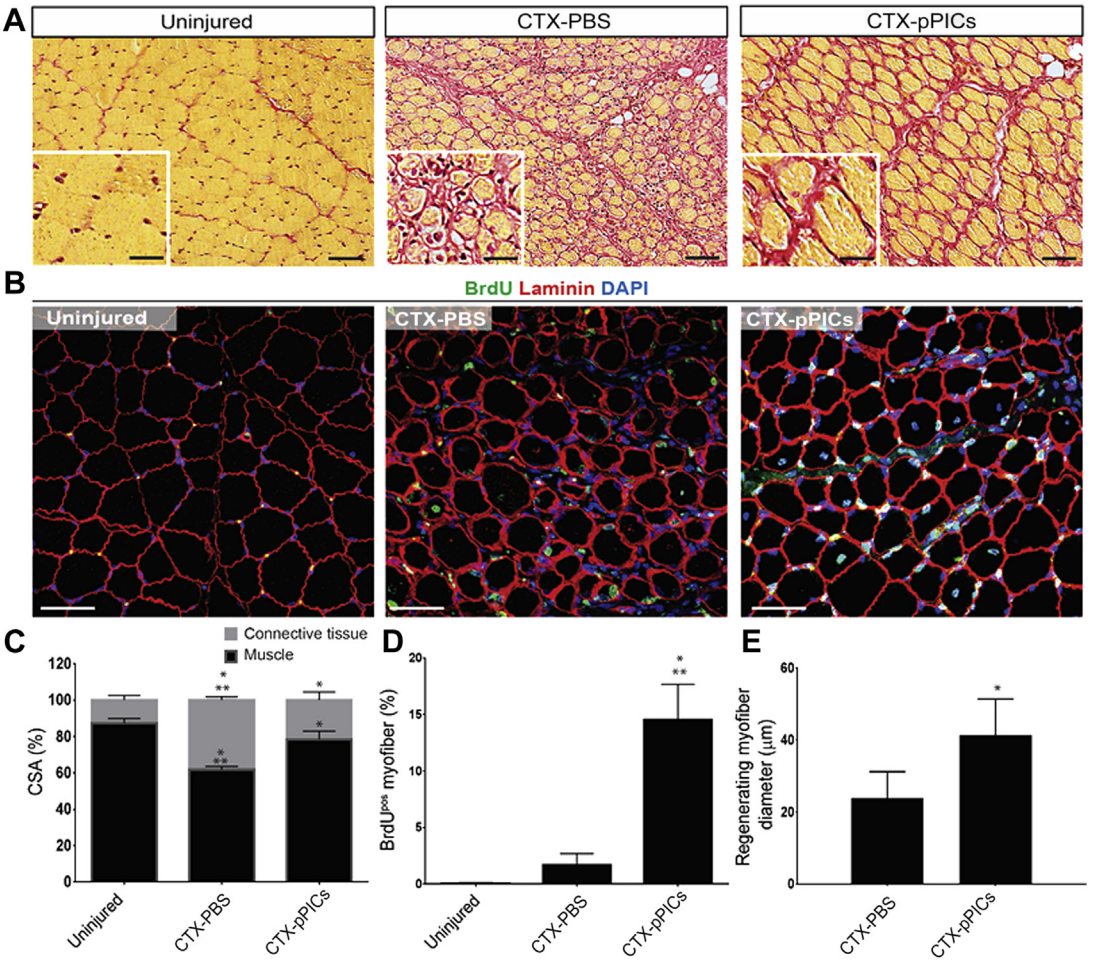

(A) HVG staining of uninjured CTRL, CTX-PBS– and CTX-pPIC–treated muscle showing improved skeletal muscle architecture in pPIC-treated muscle, scale bar = 100 μm. **Insets** show ×40 magnification, scale bar = 50 μm. **(B)** Immunohistochemical staining indicates an increase in BrdU^{pos} centralized nuclei in CTX-pPIC–treated muscle compared with uninjured CTRL and CTX-PBS–treated muscle, scale bar 50 = μm. **(C)** Quantification of the ratio of skeletal muscle to connective tissue CSA in uninjured CTRL, CTX-PBS–, and CTX-pPIC-treated muscle determined from 5 fields of view per muscle, n = 5 animals per group. Data are mean ± SD, *p < 0.01 versus uninjured CTRL, **p < 0.001 versus CTX-pPIC–treated muscle. **(D)** BrdU^{pos} centralized nuclei per total myofibers, determined from 5 fields of view per muscle, n = 5 animals per group. Data are mean ± SD, *p < 0.0001 versus uninjured CTRL, **p = 0.0012 versus CTX-PBS–treated. **(E)** Average myofiber diameter of regenerating (BrdU^{pos} centralized nuclei) myofibers determined from 5 fields of view per muscle, n = 5 animals per group. Data are mean ± SD, *p < 0.0001 versus CTX-PBS–treated. CSA = cross sectional area; CTRL = control; CTX = cardiotoxin; HVG = hematoxylin and van Gieson; PBS = phosphate buffered saline; pPIC = porcine PW1^{pos}/Pax7^{neg} interstitial cell.

PW1. No GFP^{pos} nuclei were identified beneath the basal lamina in a satellite cell position (**Figure 4A,** Supplemental Figure S4). We found only a rare occurrence of a single GFP^{pos} myofiber (per 1,000 myofibers counted) (**Figures 4A and 4B**). At 14 days post-injury, no GFPpPICs were identified in other tissues (lung, spleen, or liver) or in the uninjured contralateral control muscle (Supplemental Figure S4).

Muscle sections were stained for the infiltration of cytotoxic T cells, cytotoxic T cells/natural killer cells (NK), and macrophages expressing CD8a, Granzyme B, and IBA-1, respectively (Supplemental Figure S5). CD8a^{pos} (p = 0.0008) and Granzyme B^{pos} (p < 0.0001) cells were significantly up-regulated in CTX-pPIC–treated muscle, compared with CTX-PBS and uninjured muscle (**Figures 4C and 4D**). In terms of the innate immune cells, IBA-1-positive macrophages infiltration was significantly increased (p < 0.0004) in both CTX-PBS– and CTX-pPIC–treated muscle relative to uninjured muscle (**Figure 4E**).

FIGURE 2 Allogeneic GFP^{pos} pPICs Stimulate Neoangiogenesis Following Transplantation Into Injured Skeletal Muscle

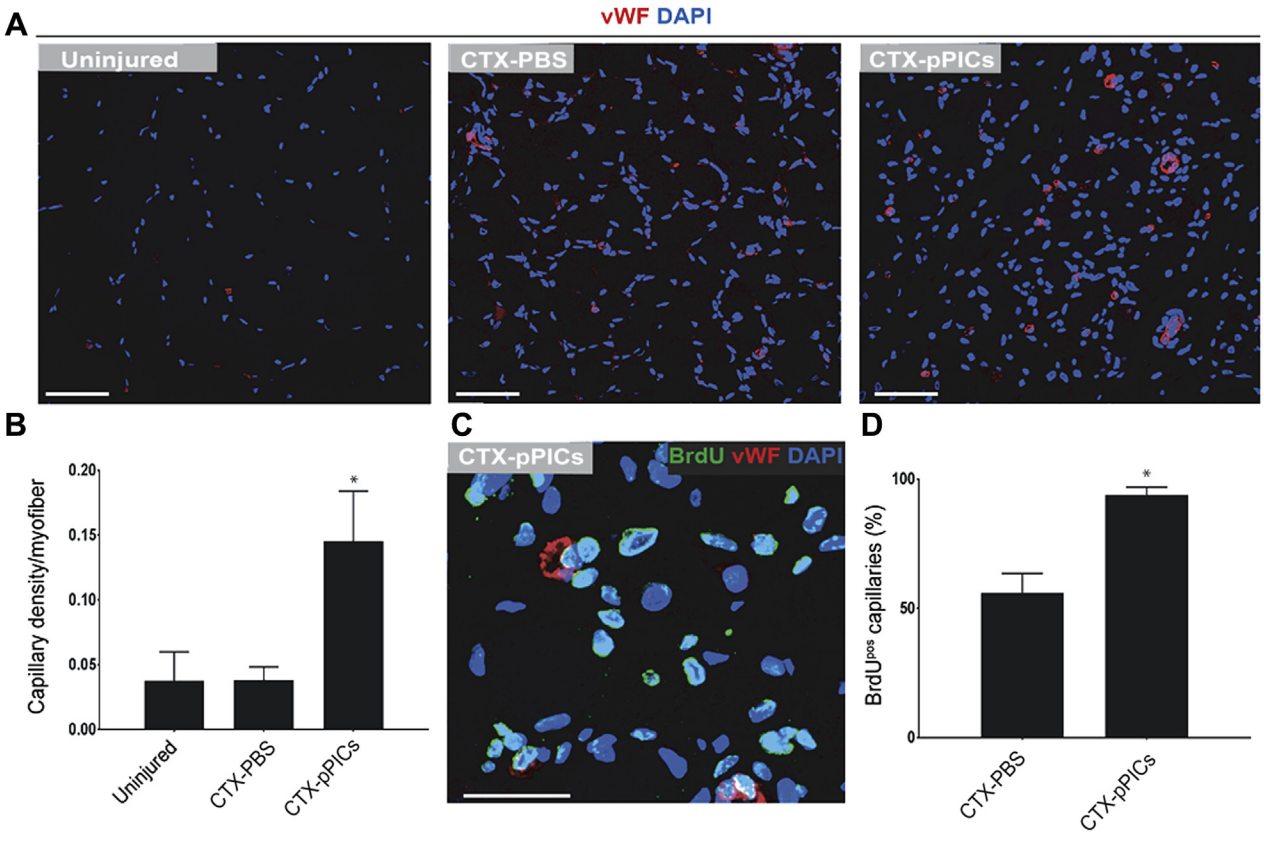

(A) Skeletal muscle cross sections were stained for vWF to evaluate capillary density, scale bar = 50 μm. **(B)** Number of capillaries per myofiber, determined from 5 fields of view per muscle, n = 5 animals per group. Data are mean ± SD, *p < 0.0001 versus uninjured. **(C)** Newly formed BrdU^{pos}/vWF^{pos} capillaries were identified 14 days post-injury, scale bar = 20 μm. **(D)** Percentage of BrdU^{pos} capillaries per total capillaries, determined from 5 fields of view per muscle, n = 5 animals per group. Data are mean ± SD, *p < 0.0001 versus CTX-PBS–treated. vWF = Von Willebrand factor; other abbreviations as in Figure 1.

To document that the immune cells (cytotoxic T cells/NK cells) were responsible for clearance of pPICs, we performed cytotoxicity assays with porcine PBMCs in vitro. Porcine PHA-activated and -inactivated PBMCs were co-cultured with pPICs at several seeding densities, and apoptosis (Annexin V/7-AAD) of pPICs was measured by flow cytometry. Activated PBMCs induced significant ($p < 0.0001$) apoptosis, between 70% and 80% in pPICs (Figure 4F). Apoptosis of pPICs did not occur when inactive PMBCs were co-cultured with pPICs (Figure 4G).

Taken together, these data suggest that allogeneic pPICs exert their action via a paracrine effect, activating endogenous progenitors before being cleared by the host immune system post-injury.

ALLOGENEIC pPICs EXPRESS AN ARRAY OF PRO-REGENERATIVE PARACRINE FACTORS. To identify the mechanism through which pPICs were able to promote regeneration in skeletal muscle, we looked to their secretome. Porcine PICs were found to express a range of cytoprotective/proregenerative growth factors and cytokines (Figure 5A), similar to that observed for stem/progenitor cells, such as mesenchymal stem cells (29) and satellite cells (30). In particular, we noted the greatest relative expression (>10,000) was chemokine (C-C Motif) ligand 2 (CCL2), monocyte chemotactic and activating factor, which is considered to be essential for stimulating muscle repair (31,32) (Figure 5A). Tissue inhibitor of metalloproteinases (TIMP)-1 and -2, involved in tissue remodeling, were also highly expressed (>100 relative expression) (Figure 5A). Factors that were 10 to 100 relative expression included those implicated in the activation, migration, proliferation, and differentiation of muscle stem/progenitor cells, such as periostin, NRG-1/2, TGF-βs, FGFs, HGF, IGF-1, INHBA, LIF, IL-6, and SCF (33–42) (Figure 5A). Interestingly,

FIGURE 3 Allogeneic GFP^{pos} pPICs Stimulate Endogenous pPIC Activation

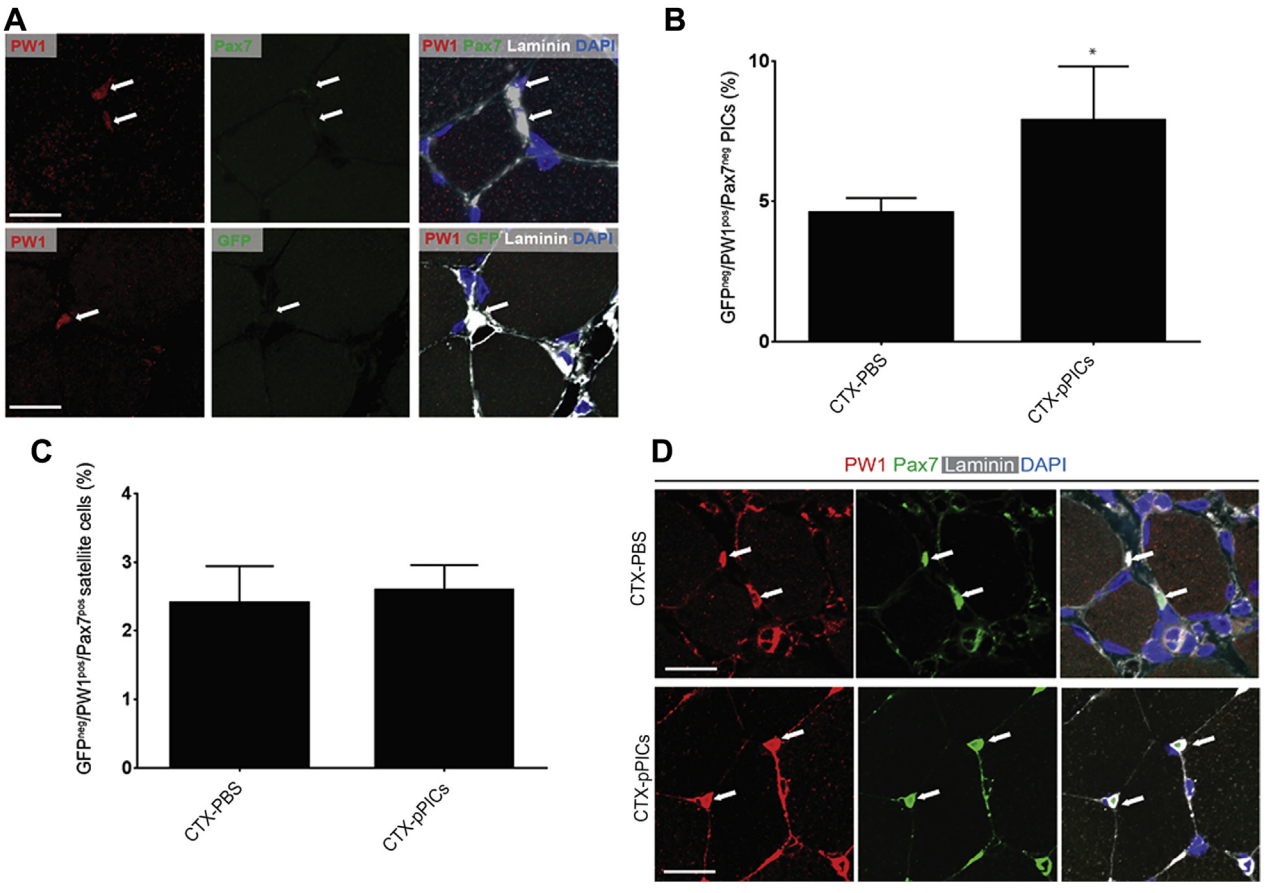

(A) Representative image of GFP^{neg}/PW1^{pos}/Pax7^{neg} pPICs resident in CTX-pPIC–treated skeletal muscle 14 days post-injury, scale bar = 50 μm. **(B)** Number of GFP^{neg}/PW1^{pos}/Pax7^{neg} pPICs per total nuclei, determined from 3 fields of view per muscle, n = 5 animals per group. Data are mean ± SD, *p = 0.0145 versus CTX-PBS–treated. **(C)** GFP^{neg}/PW1^{pos}/Pax7^{pos} satellite cells per total nuclei, determined from 3 fields of view per muscle, n = 5 animals per group. Data are mean ± SD. **(D)** Representative image of PW1^{pos}/Pax7^{pos} satellite cells resident in both CTX-PBS– and CTX-pPIC–treated skeletal muscle 14 days post-injury, scale bar = 50 μm. Abbreviations as in **Figure 1**.

GDF-11, which has been shown to ameliorate the age-related dysfunction of skeletal muscle by rescuing the function of aged muscle stem cells (43), was significantly expressed by pPICs (**Figure 5A**). Proangiogenic factors including VEGFa, PDGFs, and IL-8, capable of stimulating recruitment of endothelial cells and initiating vascularization following injury (44–46), were also found to be highly expressed (>10) in pPICs (**Figure 5A**).

To enrich for a highly paracrine secreting pPIC population, we identified whether pPICs expressed differential levels of factors depending on their differentiation status. This was necessary because following pPIC transplantation into injured skeletal muscle, the microenvironment could facilitate pPICs to differentiate into a myogenic precursor-like cell type, which could then express differential levels of proregenerative factors, compared with its undifferentiated counterpart. Therefore, a comparative qRT-PCR analysis was performed between undifferentiated pPICs and those that had undergone 24 h of myogenic differentiation in vitro (differentiated pPICs). Overall, there were distinct differences between the differentiated and undifferentiated pPICs (**Figures 5B and 5C,** Supplemental Table S1).

Volcano plot analysis highlighted factors that were significantly (>2-fold) down- or up-regulated in differentiated compared with undifferentiated pPICs (**Figure 5C,** Supplemental Table S1). Cytokines and growth factors involved in stem cell migration and proliferation, such as HGF (9), were up-regulated in undifferentiated pPICs. Whereas an up-regulation of

FIGURE 4 Allogeneic GFP^{pos} pPICs Are Cleared by the Host Immune System

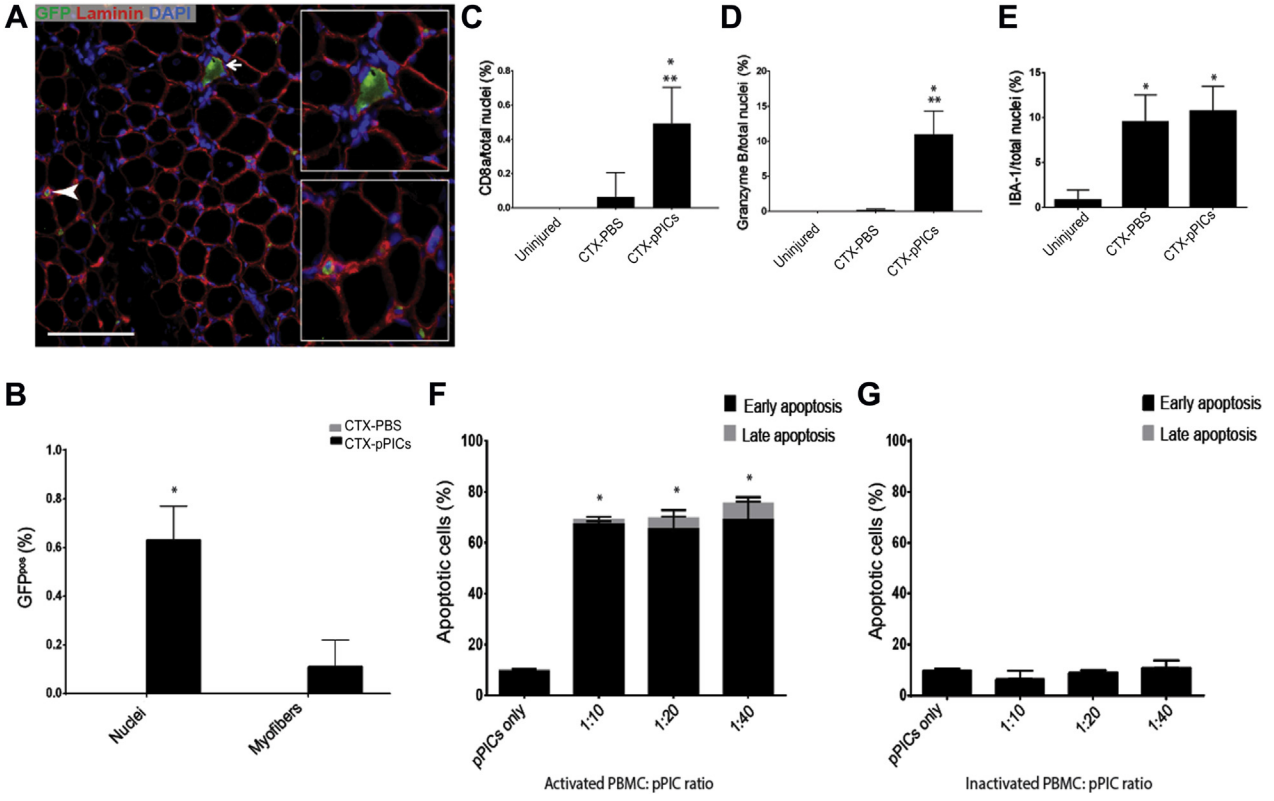

(A) Immunohistochemistry identified a small number of donor GFP^{pos} pPICs at 14 days post-transplantation, scale bar = 100 μm. GFP^{pos} cells were found as nuclei within the interstitial spaces between the muscle fibers **(bottom inset)**, and a rare GFP^{pos} muscle fiber was also identified **(top inset)**. **(B)** Quantification of GFP^{pos} cells to total number of nuclei or myofibers in paraffin embedded skeletal muscle cross sections, n = 5. Data are mean ± SD, *p = 0.001 versus CTX-PBS–treated. **(C)** Quantification of CD8^{pos} cells per total nuclei (%) determined from 5 fields of view per group. Data are mean ± SD, *p = 0.0008 versus uninjured muscle, **p = 0.0008 versus CTX-PBS–treated. **(D)** Quantification of Granzyme B^{pos} cells per total nuclei (%) determined from 5 fields of view per group. Data are mean ± SD, *p < 0.0001 versus uninjured muscle, **p < 0.0001 versus CTX-PBS–treated. **(E)** Quantification of IBA-1^{pos} cells per total nuclei (%) determined from 5 fields of view per group. Data are mean ± SD, *p = 0.0004 versus uninjured muscle. Porcine PICs were co-cultured with either **(F)** PHA-activated porcine PBMCs or **(G)** inactivated porcine PBMCs at different ratios and analyzed for apoptosis using Annexin V/7-AAD staining and flow cytometry. Early apoptosis of CD45^{neg} PICs is represented by Annexin V expression, whereas late apoptosis is represented by double-positive Annexin V/7-AAD staining, determined from duplicate wells per group. Data are mean ± SD, *p < 0.0001 versus pPICs only. PBMC = peripheral blood mononuclear cell; other abbreviations as in Figure 1.

factors involved in stem/progenitor activation and differentiation, such as INHBA, SPP-1, IL-8, BMP4, IGF-1, NRG-1, and periostin, were expressed in differentiated pPICs (Figure 5C). We confirmed changes in expression at the protein level of undifferentiated compared with differentiated pPICS for a selected panel of up- or down-regulated factors, which supported the transcript data (Figure 5D). These data suggest that both undifferentiated and differentiated pPICs could be used to exert a pro-regenerative paracrine effect, but differentiated pPICs up-regulate expression of a vaster array of proregenerative factors.

THE pPIC SECRETOME PROMOTES A REGENERATIVE RESPONSE IN VITRO. We next examined the effect of the pPIC secretome on human myoblast and pPIC proliferation and differentiation in vitro. CM significantly ($p < 0.0001$) increased proliferation of pPICs (Figure 6A) and myoblasts (Figure 6B), compared with UM and ICM where the secreted factors were absent or denatured, respectively (Figures 6A and 6B). Next, we showed that factors that were expressed by pPICs, such as IGF-1, HGF, and NRG-1, when supplemented to pPICs in vitro, significantly ($p < 0.0001$) increased their proliferation (Figure 6C), and for TGF-β1, increased pPIC differentiation (Figures 6D and 6E)

assessed by quantifying the fusion index of MHC^{pos} cells, compared with unsupplemented control. Moreover, in vitro angiogenesis assays confirmed that secreted factors in CM promoted HUVECs to form endothelial networks, evidenced by a significant increase in capillary area ($p = 0.0189$) and total tube length ($p = 0.0224$) compared with ICM (**Figures 6F and 6G,** Supplemental Figure S5). Taken together, these data demonstrate that factors secreted by pPICs promote proliferation and differentiation of skeletal muscle progenitors and stimulate angiogenesis in vitro.

ADMINISTRATION OF HGF AND IGF-1 IMPROVES SKELETAL MUSCLE REGENERATION, BUT NOT TO THE SAME EXTENT AS pPIC TRANSPLANTATION. To determine whether cytokines produced by other cell types other than pPICs could contribute to repair, we immunostained muscle sections for 4 growth factors, IGF-1, HGF, TGF-β1, and NRG1. CTX-pPIC–treated transplanted muscle showed increased expression of all factors, compared with CTX-PBS–treated and uninjured muscle. Specifically, HGF expression was mainly confined to the myofibers; IGF-1 and NRG1 expression was confined to the myofibers and interstitial cells, and TGFβ1 expression was confined to the interstitial cells, following CTX-pPIC–treated transplantation (Supplemental Figure S7).

To determine whether IGF-1 and HGF could improve regeneration to a similar degree as pPIC transplantation, we injected IGF-1 and HGF into CTX-injured skeletal muscle, and we also administered the same growth factors through a UPy hydrogel, as we have done previously in the porcine chronic MI model (47). We found that IGF-1/HGF administration improved muscle regeneration, increasing the number of $BrdU^{pos}$ myofibers ($8 \pm 2\%$/total myofibers vs. $2 \pm 1\%$/total myofibers CTX-PBS–treated) and the $BrdU^{pos}$ regenerating myofibers were larger (33.28 ± 6.3 μm vs. 23.8 ± 7.3 μm CTX-PBS–treated) (**Figure 7**). However, these effects were not further enhanced if the growth factors were administered through the UPy hydrogel ($BrdU^{pos}$ myofiber $8 \pm 3\%$/total myofibers and $BrdU^{pos}$ regenerating myofibers diameter 35.58 ± 4.98 μm), and more importantly, the improvements were not as great as transplantation of pPICs (**Figure 1**). Therefore, pPICs are superior to targeted growth factor administration because they release a plethora of growth factors and cytokines, which activate multiple endogenous repair mechanisms, contributing to accelerated and effective repair and regeneration in vivo.

DISCUSSION

The present study documents that in a porcine model of skeletal muscle damage, which is applicable to humans, transplantation of allogeneic pPICs persist long enough to elicit a paracrine effect by secretion of regenerative cytokines and growth factors. These factors stimulate endogenous progenitor cell activation and differentiation, leading to accelerated and improved autologous myofiber regeneration and microvessel formation.

Skeletal muscle, although capable of undergoing extensive regeneration, exhibits diminished regenerative capacity in ageing and disease. The loss of regenerative capacity is largely thought to be due to intrinsic and extrinsic changes that ultimately abrogate resident progenitor cell competence (48,49). Intrinsic mechanisms include epigenetic changes, telomere attrition, DNA damage or mitochondrial dysfunction. Extrinsic changes are associated with alterations of the muscle progenitor cell niche, which can be influenced by both systemic circulating factors and local changes associated with ageing, disease or metabolic pathways, which can negatively impact endogenous progenitor cells.

To date, most attempts to regenerate skeletal muscle have focused on delivery of culture-expanded myoblasts (50) or $CD133^{pos}$ cells (51), which have been shown to engraft and generate functional satellite cells after xenotransplantation in rodent models, suggesting the potential for autologous regenerative applications. Despite advances, the results of clinical trials (52,53) collectively show low engraftment efficiency with prevailing issues associated with immune rejection. Over recent years, a large number of reports have shown that transplanted stem cells mediate their beneficial effects via several indirect mechanisms, such as recruitment of endogenous progenitor cells, induction of angiogenesis, protection of existing survived cells and reduction in fibrosis and inflammation (9,54). These processes are regulated by a variety of small molecules, proteins, mRNAs/miRNAs, and paracrine factors produced by the adoptively transferred stem cells in the damaged tissue milieu (54–56). This concept has been prevalent for many years, where it was shown the infusion of human umbilical cord blood cells can aid in stroke recovery due to enhanced angiogenesis, which may have induced neuroblast migration to the site of injury (57). Moreover, transplanted macrophages can promote liver repair by activating hepatic progenitor cells (58). We have previously documented the protective and regenerative effects of allogeneic CSCs transplantation or growth factor administration in porcine models of MI (9,12). CSCs express high levels of numerous cytokines, including chemokines (TCA-3, SDF-1, 6Ckine), vascular growth factors (VEGF, EPO, bFGF, SCF), survival and activation

FIGURE 5 Allogeneic pPICs Express an Array of Proregenerative Paracrine Factors

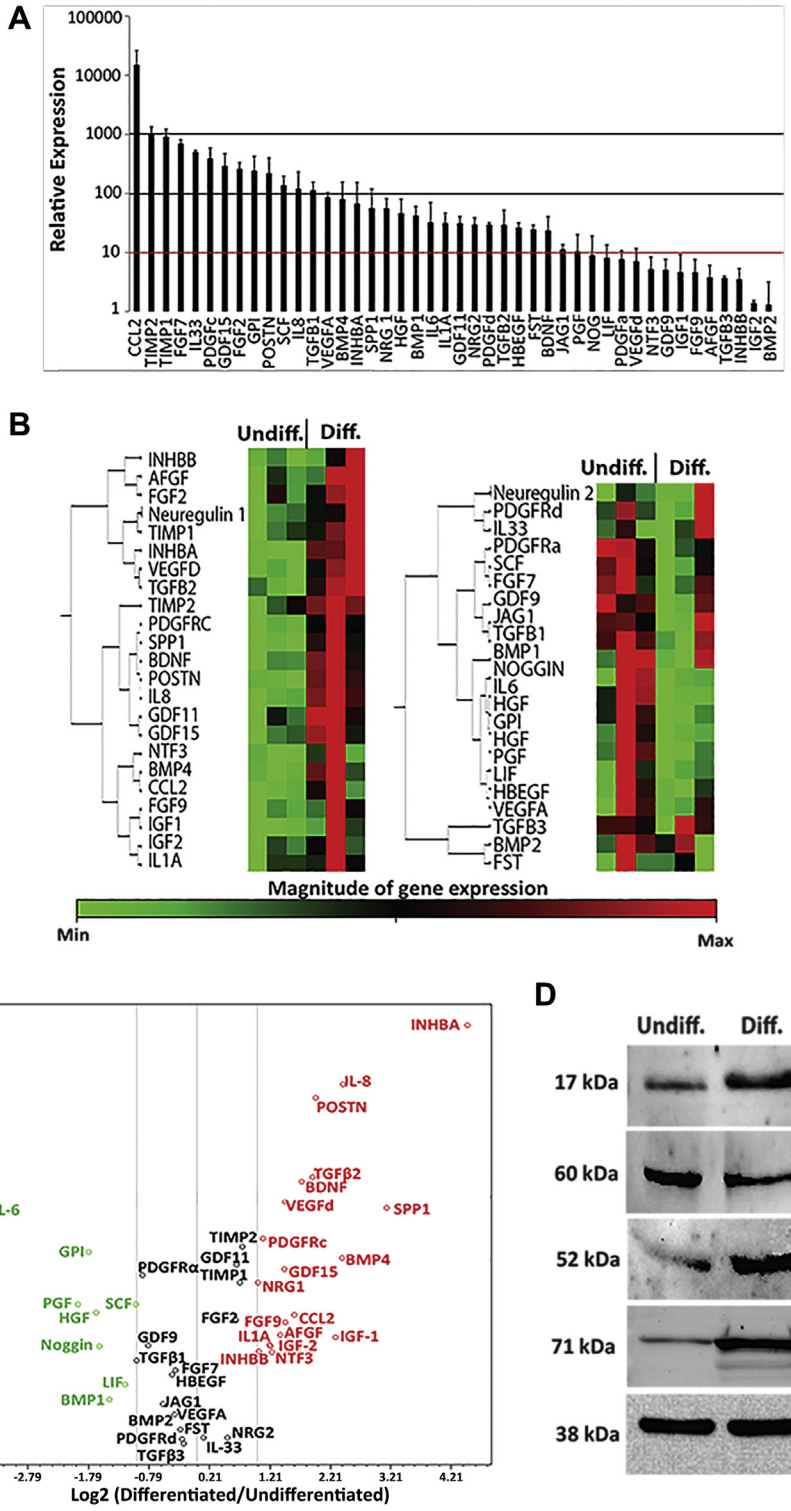

Continued on the next page

factors (IGF-1, HGF, PDGFs), and cardiac differentiation factors (Activin A, Dkk-1, TGF-β), which are released at the site of injury, activating endogenous repair mechanisms and improving cardiac function (9,12,59,60).

To our knowledge, this is the first study to show that allogeneic stem/progenitor cell transplantation elicits a paracrine effect by activating endogenous repair processes to improve and accelerate muscle regeneration in the pig. To date preclinical studies have not addressed the magnitude of the regeneration required to target whole skeletal muscle regeneration in the clinic. The best published results report regeneration in the region of milligrams of skeletal muscle in small mouse animal models, whereas humans would likely require at least a 3-fold increase in muscle mass in comparison (61). Here, we developed a large animal, preclinical skeletal muscle injury model, which is easily reproducible and is a useful, clinically applicable model to assess the effects of proof-of-concept regenerative therapies designed to regenerate large volumes of muscle. The animals that were used were juvenile animals, ~2-month-old pigs, which were selected due to their reduced size and practicability issues. They also had a functioning immune system required to test our theory that transplanted pPICs would be cleared by the host immune system. We showed that transplanted pPICs were cleared from the host by 14 days post-transplantation, and activated porcine PMBCs effectively killed pPICs in a cytotoxicity assay in vitro. Analysis of the immune response revealed that CTX-pPIC-treated muscle had increased CD8a (adaptive immunity) and Granzyme B (adaptive/innate immunity) cells and both CTX-PBS- and CTX-pPIC-treated muscle had comparable infiltration of macrophages that were significantly greater than in uninjured muscle. On the basis of these results, we propose that the donor pPICs were removed in the early phases of regeneration, and the increased regenerative response was mediated as a consequence of the activated endogenous progenitors.

Transplantation of allogeneic pPICs was found to stimulate the endogenous repair mechanisms of this tissue, leading to improved and accelerated skeletal muscle regeneration, with increased muscle CSA, an increased number of $BrdU^{pos}$ centralized nuclei, and larger regenerating myofibers compared with CTX-PBS-treated muscle. In addition to myofiber regeneration following muscle trauma, damaged blood vessels lead to tissue hypoxia at the injury site (62); therefore, new capillary formation after injury is also necessary for functional muscle recovery (63). Secretion of angiogenic factors, such as VEGF, at the injury site is an important mediator of this process, and several studies have shown that VEGF improves skeletal muscle repair by promoting angiogenesis (44,64). This study identified that following allogeneic pPIC transplantation, there was a significant increase in new capillary formation, which would have contributed to the improvement in muscle regeneration observed.

Allogeneic pPIC treatment was shown to activate and increase the number of endogenous $PW1^{pos}$/$Pax7^{neg}$ PICs, yet a similar increase in number was not found for $PW1^{pos}$/$Pax7^{pos}$ satellite cells. Therefore, pPICs may either have a greater stimulatory effect on the endogenous PICs, or more likely, the time point of 14 days is insufficient to accurately measure the effect of pPIC transplantation on satellite cell activation. Because satellite cells are the main contributor to muscle regeneration (65), it is likely that the satellite cells became activated early (days 1 to 3) and had returned to normal, quiescent levels once the regeneration process was almost complete at 14 days. Moreover, the assessment of satellite cell activation is hampered by lack of markers to identify activated satellite cells in the interstitial space (30). Also, the endogenous PICs might have maintained an activated state for longer due to their role in vascular repair.

FIGURE 5 Continued

(A) Expression profile of pPICs arrayed by quantitative reverse transcription polymerase chain reaction, relative expression to average expression of 5 housekeeping genes *ACTB*, *B2M*, *GAPDH*, *HPRT1*, and *RPL13A*. Data represent mean ± SD, n = 3. **(B)** Hierarchical clustering of differentially regulated pPIC transcripts. The colors in ascending order from **green to red** represent the magnitude of gene expression for the measured average difference values. The tree on the **left** of the clustergram indicates the pairwise similarity relationships between the clustered expression patterns, n = 3 for both undifferentiated and differentiated pPICs (24 h in differentiation medium). **(C)** Genes that were differentially regulated by at least 2-fold were selected and are illustrated in a volcano plot. **Red** indicates those genes that were up-regulated, **black** represents genes whose expression levels did not change, whereas **green** indicates genes that were down-regulated in differentiated pPICs compared with undifferentiated pPICs, n = 3. **(D)** Western blots confirmed that pPIC exposure to a myogenic permissive environment led to an increase in IGF-1, TGF-β1, and NRG-1, and a decrease in HGF protein expression, n = 3. Diff = differentiated; pPIC = porcine $PW1^{pos}$/$Pax7^{neg}$ interstitial cell; Undiff = undifferentiated.

FIGURE 6 The pPIC Secretome Promotes a Regenerative Response in Vitro

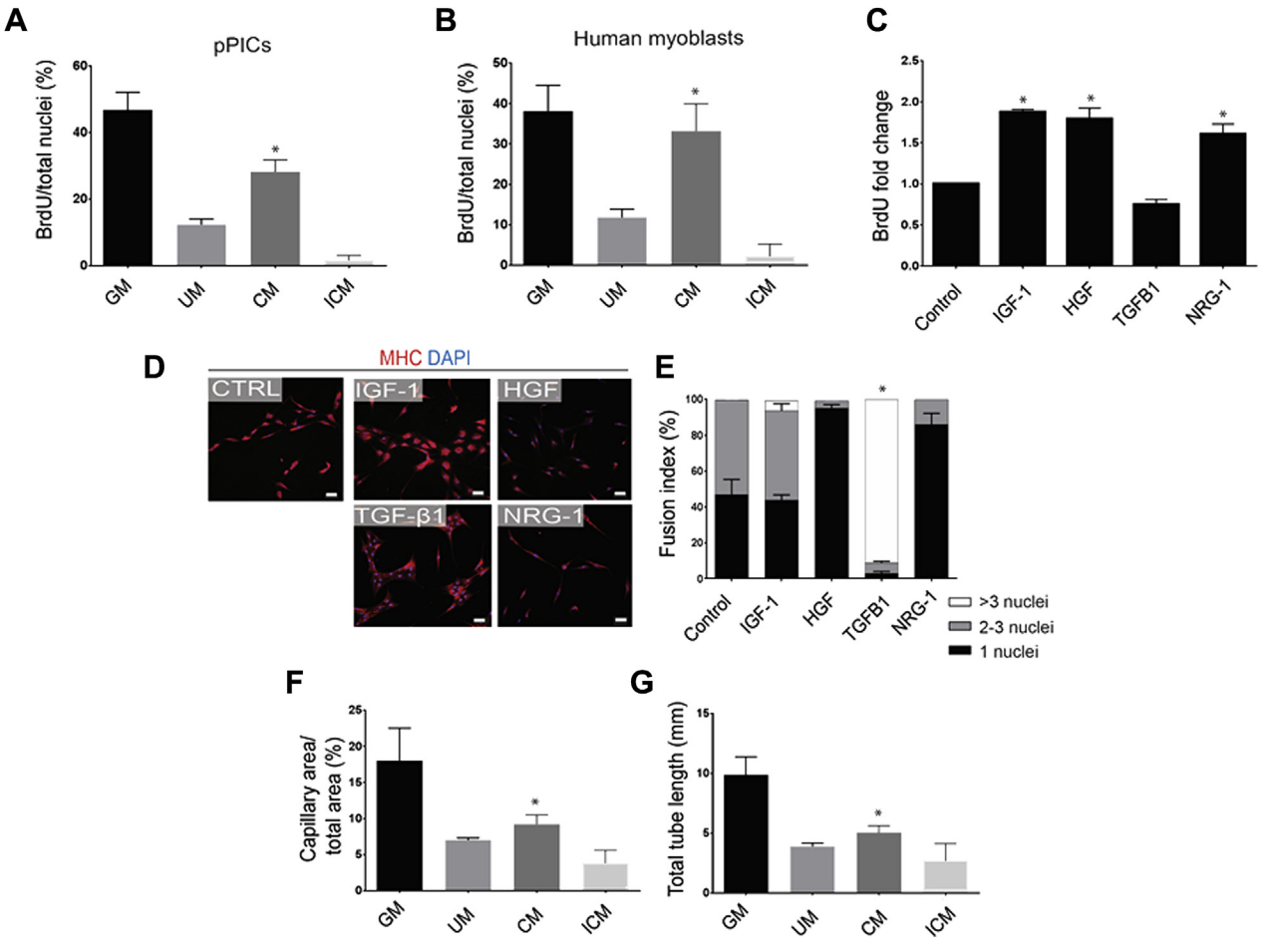

(A) Quantification of pPIC BrdU 24-h proliferation assay in standard growth media (GM), 24-h pPIC conditioned media (CM), unconditioned media (UM), or heat-inactivated conditioned media (ICM). Total $BrdU^{pos}$ cells per total nuclei, determined from 5 fields of view per group. Data are mean ± SD, *$p < 0.0001$ versus all conditions. **(B)** Quantification of human myoblasts BrdU 24-h proliferation assay in GM, CM, UM, or ICM. Total $BrdU^{pos}$ cells per total nuclei, determined from 5 fields of view per group. Data are mean ± SD, *$p < 0.0001$ versus UM and ICM. **(C)** Quantification of BrdU 24-h proliferation assay in medium supplemented with IGF-1, HGF, TGF-β1, or NRG-1 compared with control. Total $BrdU^{pos}$ cells per total nuclei, determined from 5 fields of view per group. Data are mean ± SD, *$p < 0.0001$ versus control and TGF-β1. **(D)** Representative micrographs of pPIC immunocytochemical staining for MHC after 5 days of myogenic differentiation in the presence of IGF-1, HGF, NRG-1, or TGF-β1 compared with control. **(E)** Quantification of pPIC fusion index after 5 days of myogenic differentiation in the presence of IGF-1, HGF, TGF-β1, or NRG-1 compared with control. Data are mean ± SD, *$p < 0.0001$ versus control for >3 nuclei. **(F and G)** Endothelial network formation quantified as capillary area **(F)** and total length of capillaries **(G)**, after human umbilical vein endothelial cells were exposed to endothelial GM, CM, UM, and ICM. Data are mean ± SD, *$p < 0.05$ versus ICM and GM. MHC = myosin heavy chain; other abbreviations as in Figure 1.

However, these data suggest the existence of a feedback loop triggered by the transplanted pPICs that activates the production of growth and survival factors by the endogenous PICs, which could explain their persistence and longer duration of activation over 14 days. The relationship between satellite cells and endogenous PICs during the repair and regeneration of skeletal muscle thus warrants further investigation.

We determined whether the paracrine effect of pPICs depended on their differentiation status, and predicted that upon transplantation, the in vivo microenvironment encountered by the pPICs during the first 24 h would promote pPIC differentiation. The secretome of 24-h differentiated pPICs showed increased expression of factors, such as IGF-1, NRG-1, and TGF-β1 and periostin, which facilitated proliferation and differentiation of endogenous muscle stem/

FIGURE 7 Administration of IGF-1/HGF and UPy IGF-1/HGF Stimulates Moderate Skeletal Muscle Regeneration

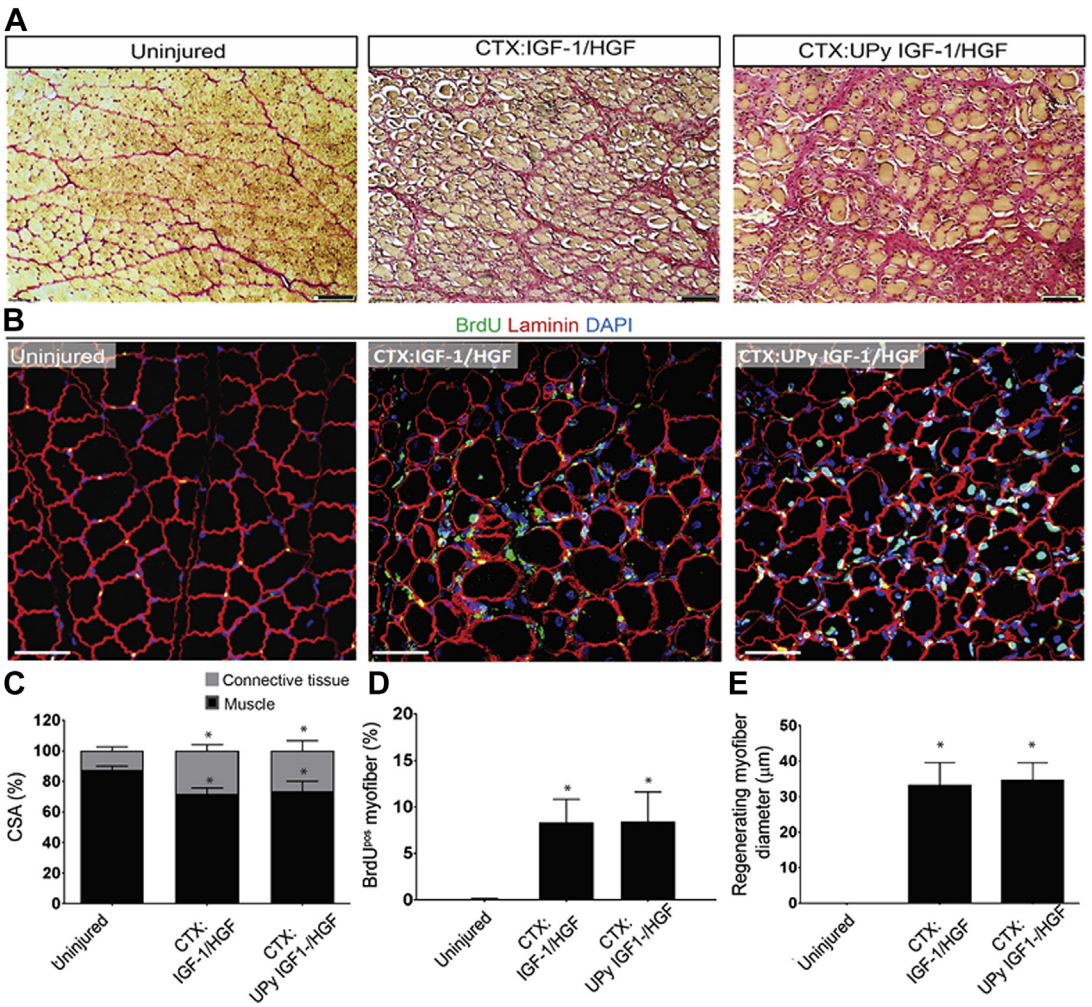

(A) HVG staining of uninjured, CTX:IGF-1/HGF–, and CTX:UPy IGF-1/HGF–treated muscle, scale bar = 100 μm. **(B)** Immunohistochemical staining shows a number of $BrdU^{pos}$ centralized nuclei in both CTX:IGF-1/HGF– and CTX:UPy IGF-1/HGF–treated muscle compared with uninjured muscle, scale bar = 50 μm. **(C)** Quantification of the ratio of skeletal muscle to connective tissue CSA in uninjured, CTX:IGF-1/HGF–, and CTX:UPy IGF-1/HGF–treated muscle determined from 5 fields of view per muscle, n = 5 animals per group. Data are mean ± SD, *p < 0.01 versus uninjured CTRL. **(D)** $BrdU^{pos}$ centralized nuclei per total myofibers, determined from five fields of view per muscle, n = 5 animals per group. Data are mean ± SD, *p < 0.001 versus uninjured CTRL. **(E)** Average myofiber diameter of regenerating ($BrdU^{pos}$ centralized nuclei) myofibers determined from 5 fields of view per muscle, n = 5 animals per group. Data are mean ± SD, *p < 0.0001 versus uninjured CTRL. Abbreviations as in Figure 1.

progenitor cells. In vitro assays confirmed that conditioned media containing these secreted factors stimulated the proliferation of both pPICs and human myoblasts, and stimulated endothelial network formation of HUVECs. Moreover, IGF-1, HGF, and NRG-1, when supplemented individually to the culture media, stimulated the proliferation of pPICs, whereas TGF-β1 was shown to play a role in promoting pPIC myogenic differentiation. Therefore, allogeneic pPIC transplantation elicits a paracrine effect on endogenous progenitor cells, increasing and accelerating skeletal muscle regeneration.

Many different stem/progenitor cells (66-72) have been investigated for cellular therapy, each with their

own set of unique advantages and shortcomings. Given the striated muscle similarities between skeletal and cardiac muscle, skeletal muscle-derived myoblasts were the first cell type to enter the clinical arena of heart repair (73). Skeletal muscle-derived progenitors showed promise in that they were proangiogenic and relatively resistant to hypoxic conditions, and therefore improved functional outcomes upon transplantation (74,75). However, due to issues associated with limited expansion in vitro and arrhythmogenic complications in vivo (76), they are widely considered unsuitable for cardiac regeneration. Utilizing PICs as a source of stem/progenitor cells for allogeneic cell therapy overcomes several of the limitations encountered with other adult muscle progenitor therapies and mesenchymal allogeneic therapies. Indeed, harvesting of PICs from an easily accessible source, such as skeletal muscle, means a simple muscle biopsy would be performed, and with an unlimited proliferative capacity in vitro, a large number can be propagated, maintaining a stable phenotype and genotype over passage number (16). Together with a rich secretome of regenerative factors, these properties make PICs an ideal candidate cell source for the repair of the heart as well as other tissues.

STUDY LIMITATIONS. One of the main limitations associated with the clinical application of stem cell-based therapies is the time and costs associated with generating the large number of clinical grade cells required for treatment. Therefore, it may be beneficial to assess the effect of different doses of pPICs to ascertain whether fewer cells could stimulate the same effect. Nevertheless, we envision the main advancement of these findings to be in identifying specific factors responsible for eliciting accelerated and improved muscle and microvessel regeneration. This would enable us to develop cell-free therapies that match or exceed the level of regeneration reported here, which would greatly facilitate clinical application. However, the delivery of HGF and IGF-1 to the injured skeletal muscle did not result in equivalent levels of muscle regeneration documented for pPIC transplantation. Therefore, delivery of a multitude of factors/molecules is necessary, at different time points after injury, to elicit optimal repair and regeneration of the tissue.

Another limitation of this study is the unknown effect of transplanting PICs into diseased muscle, such as diabetes or muscular dystrophy models, where the harsh environment and metabolic elements affect stromal stem cell activity and potency (77). Moving toward clinical application, this warrants investigation because we may require a combinatorial approach in order to overcome the harsh environments that the transplanted PICs will likely encounter.

CONCLUSIONS

Taken together, these results provide the proof of concept needed to justify further experimental development and refinement of this allogeneic cell therapy approach, which ultimately could lead to an effective, simple, clinically applicable, and widely available protocol of tissue repair and regeneration.

ACKNOWLEDGMENTS The authors thank the following persons for their technical assistance with the animal experiments: S. Koudstaal, S. Jansen of Lorkeers, and P. Zwetsloot; C. Hobbs for his technical assistance with the processing and staining of porcine tissue sections; and D. Burch and M. Nevel for providing pig blood to isolate PBMCs.

ADDRESS FOR CORRESPONDENCE: Dr. Georgina M. Ellison-Hughes, School of Basic and Medical Biosciences, Faculty of Life Sciences & Medicine, King's College London, Shepherd's House, Room 4.16, Guy's Campus, London SE1 1UL, United Kingdom. E-mail: georgina.ellison@kcl.ac.uk.

PERSPECTIVES

COMPETENCY IN MEDICAL KNOWLEDGE: Allogeneic PIC transplantation elicits a paracrine effect through secretion of regenerative cytokines and growth factors, which stimulate endogenous progenitor cell activation and differentiation, leading to accelerated and improved myofiber regeneration and microvessel formation. Shortly after they have elicited their paracrine effect, they are removed by the host immune system. This allogeneic cell approach is considered an off-the-shelf, cost-effective, easy-to-apply, and readily-available regenerative therapeutic strategy.

TRANSLATIONAL OUTLOOK: This study provides a proof-of-concept for an allogeneic cell therapy approach, which with further experimental development and refinement may lead to an effective, simple, clinically applicable, and widely available strategy for repair of the heart and other organs.

REFERENCES

1. Ciciliot S, Schiaffino S. Regeneration of mammalian skeletal muscle. Basic mechanisms and clinical implications. Curr Pharm Des 2010;16:906–14.

2. Karpati G, Molnar MJ. Muscle fibre regeneration in human skeletal muscle diseases. In: Schiaffino S, Partridge T, editors. Skeletal Muscle Repair and Regeneration: Advances in Muscle Research, Volume 3. Dordrecht, the Netherlands: Springer, 2008:199–216.

3. Brack AS, Rando TA. Age-dependent changes in skeletal muscle regeneration. In: Schiaffino S, Partridge T, editors. Skeletal Muscle Repair and Regeneration: Advances in Muscle Research, Volume 3. Dordrecht, the Netherlands: Springer, 2008:359–74.

4. Mann CJ, Perdiguero E, Kharraz Y, et al. Aberrant repair and fibrosis development in skeletal muscle. Skelet Muscle 2011;1:21.

5. Degens H. Age-related changes in the microcirculation of skeletal muscle. Adv Exp Med Biol 1998;454:343–8.

6. Brack AS, Rando TA. Intrinsic changes and extrinsic influences of myogenic stem cell function during aging. Stem Cell Rev 2007;3:226–37.

7. Conboy IM, Al-Shanti N, Lewis MP, Stewart CE. Rejuvenation of aged progenitor cells by exposure to a young systemic environment. Nature 2005;433:760–4.

8. Ceafalan LC, Popescu BO, Hinescu ME. Cellular players in skeletal muscle regeneration. Biomed Res Int 2014;2014:957014.

9. Ellison GM, Torella D, Dellegrottaglie S, et al. Endogenous cardiac stem cell activation by insulin-like growth factor-1/hepatocyte growth factor intracoronary injection fosters survival and regeneration of the infarcted pig heart. J Am Coll Cardiol 2011;58:977–86.

10. Madrigal M, Rao KS, Riordan NH. A review of therapeutic effects of mesenchymal stem cell secretions and induction of secretory modification by different culture methods. J Transl Med 2014;12:260.

11. Mason C, Dunnill P. Assessing the value of autologous and allogeneic cells for regenerative medicine. Regen Med 2009;4:835–53.

12. Ellison GM, Nadal-Ginard B, Torella D. Optimizing cardiac repair and regeneration through activation of the endogenous cardiac stem cell compartment. J Cardiovasc Transl Res 2012;5:667–77.

13. Tedesco FS, Dellavalle A, Diaz-Manera J, Messina G, Cossu G. Repairing skeletal muscle: regenerative potential of skeletal muscle stem cells. J Clin Invest 2010;120:11–9.

14. Ding S, Wang F, Liu Y, Li S, Zhou G, Hu P. Characterization and isolation of highly purified porcine satellite cells. Cell Death Discov 2017;3:17003.

15. Mitchell KJ, Pannérec A, Cadot B, et al. Identification and characterization of a non-satellite cell muscle resident progenitor during postnatal development. Nat Cell Biol 2010;12:257–66.

16. Lewis FC, Henning BJ, Marazzi G, Sassoon D, Ellison GM, Nadal-Ginard B. Porcine skeletal muscle-derived multipotent PW1pos/Pax7neg interstitial cells: isolation, characterization and long-term culture. Stem Cells Transl Med 2014;3:702–12.

17. Swindle MM, Makin A, Herron AJ, Clubb FJ, Frazier KS. Swine as models in biomedical research and toxicology testing. Vet Pathol 2012;49:344–56.

18. Toniolo L, Patruno M, Maccatrozzo L, et al. Fast fibres in a large animal: fibre types, contractile properties and myosin expression in pig skeletal muscles. J Exp Biol 2004;207 Pt 11:1875–86.

19. Hakimov HA, Walters S, Wright TC, et al. Application of iTRAQ to catalogue the skeletal muscle proteome in pigs and assessment of effects of gender and diet dephytinization. Proteomics 2009;9:4000–16.

20. Lefaucheur L, Ecolan P, Plantard L, Gueguen N. New insights into muscle fiber types in the pig. J Histochem Cytochem 2002;50:719–30.

21. Orlic D, Kajstura J, Chimenti S, et al. Bone marrow cells regenerate infarcted myocardium. Nature 2001;410:701–5.

22. Gussoni E, Soneoka Y, Strickland CD, et al. Dystrophin expression in the mdx mouse restored by stem cell transplantation. Nature 1999;401:390–4.

23. Afzal MR, Samanta A, Shah ZI, et al. Adult bone marrow cell therapy for ischemic heart disease: evidence and insights from randomized controlled trials. Circ Res 2015;117:558–75.

24. Leung DG, Wagner KR. Therapeutic advances in muscular dystrophy. Ann Neurol 2013;74:404–11.

25. Bastings MM, Koudstaal S, Kieltyka RE, et al. A fast pH-switchable and self-healing supramolecular hydrogel carrier for guided, local catheter injection in the infarcted myocardium. Adv Healthc Mater 2014;3:70–8.

26. Agley CC, Rowlerson AM, Velloso CP, Lazarus NL, Harridge SD. Isolation and quantitative immunocytochemical characterization of primary myogenic cells and fibroblasts from human skeletal muscle. J Vis Exp 2015;95:52049.

27. Bancroft JD, Cook HC. Manual of Histological Techniques. New York, NY: Churchill Livingstone, 1984.

28. Czerwinska AM, Streminska W, Ciemerych MA, Grabowska I. Mouse gastrocnemius muscle regeneration after mechanical or cardiotoxin injury. Folia Histochem Cytobiol 2012;50:144–53.

29. Ranganath SH, Levy O, Inamdar MS, Karp JM. Harnessing the mesenchymal stem cell secretome for the treatment of cardiovascular disease. Cell Stem Cell 2012;10:244–58.

30. Yin H, Price F, Rudnicki MA. Satellite cells and the muscle stem cell niche. Physiol Rev 2013;93:23–67.

31. Lu H, Huang D, Ransohoff RM, Zhou L. Acute skeletal muscle injury: CCL2 expression by both monocytes and injured muscle is required for repair. FASEB J 2011;25:3344–55.

32. Hirata A, Masuda S, Tamura T, et al. Expression profiling of cytokines and related genes in regenerating skeletal muscle after cardiotoxin injection: a role for osteopontin. Am J Pathol 2003;163:203–15.

33. Ozdemir C, Akpulat U, Sharafi P, Yıldız Y, Onbaşılar I, Kocaefe C. Periostin is temporally expressed as an extracellular matrix component in skeletal muscle regeneration and differentiation. Gene 2014;553:130–9.

34. Hirata M, Sakuma K, Okajima S, et al. Increased expression of neuregulin-1 in differentiating muscle satellite cells and in motoneurons during muscle regeneration. Acta Neuropathol 2007;113:451–9.

35. Kim HO, Choi S, Kim H. Mesenchymal stem cell-derived secretome and microvesicles as a cell-free therapeutics for neurodegenerative disorders. J Tissue Eng Regen Med 2013;10:93–101.

36. Bentzinger CF, Wang YX, Rudnicki MA. Building muscle: molecular regulation of myogenesis. Cold Spring Harb Perspect Biol 2012;4:a008342.

37. Guo X, Chen S. Transforming growth factor-β and smooth muscle differentiation. World J Biol Chem 2012;3:41–52.

38. Song YH, Song JL, Delafontaine P, Godard MP. The therapeutic potential of IGF-I in skeletal muscle repair. Trends Endocrinol Metab 2013;24:310–9.

39. Broholm C, Pedersen BK. Leukaemia inhibitory factor–an exercise-induced myokine. Exerc Immunol Rev 2010;16:77–85.

40. Serrano AL, Baeza-Raja B, Perdiguero E, Jardí M, Muñoz-Cánoves P. Interleukin-6 is an essential regulator of satellite cell-mediated skeletal muscle hypertrophy. Cell Metab 2008;7:33–44.

41. Zhang C, Li Y, Wu Y, Wang L, Wang X, Du J. Interleukin-6/signal transducer and activator of transcription 3 (STAT3) pathway is essential for macrophage infiltration and myoblast proliferation during muscle regeneration. J Biol Chem 2013;288:1489–99.

42. Huang Z, Ruan HB, Xian L, et al. The stem cell factor/Kit signalling pathway regulates mitochondrial function and energy expenditure. Nat Commun 2014;5:4282.

43. Sinha M, Jang YC, Oh J, et al. Restoring systemic GDF11 levels reverses age-related dysfunction in mouse skeletal muscle. Science 2014;344:649–52.

44. Deasy BM, Feduska JM, Payne TR, Li Y, Ambrosio F, Huard J. Effect of VEGF on the regenerative capacity of muscle stem cells in dystrophic skeletal muscle. Mol Ther 2009;17:1788–98.

45. Moriya J, Wu X, Zavala-Solorio J, Ross J, Liang XH, Ferrara N. Platelet-derived growth factor C promotes revascularization in ischemic limbs of diabetic mice. J Vasc Surg 2014;59:1402–9.e1–4.

46. Bouïs D, Kusumanto Y, Meijer C, Mulder NH, Hospers GA. A review on pro- and anti-angiogenic factors as targets of clinical intervention. Pharmacol Res 2006;53:89–103.

47. Koudstaal S, Bastings MM, Feyen DA, et al. Sustained delivery of insulin-like growth factor-1/hepatocyte growth factor stimulates endogenous cardiac repair in the chronic infarcted pig heart. J Cardiovasc Transl Res 2014;7:232–41.

48. Didier N, Hourdé C, Amthor H, Marazzi G, Sassoon D. Loss of a single allele for Ku80 leads to progenitor dysfunction and accelerated aging in skeletal muscle. EMBO Mol Med 2012;4:910–23.

49. Gopinath SD, Rando TA. Stem cell review series: aging of the skeletal muscle stem cell niche. Aging Cell 2008;7:590–8.

50. Skuk D, Paradis M, Goulet M, Chapdelaine P, Rothstein DM, Tremblay JP. Intramuscular transplantation of human postnatal myoblasts generates functional donor-derived satellite cells. Mol Ther 2010;18:1689–97.

51. Meng J, Chun S, Asfahani R, Lochmüller H, Muntoni F, Morgan J. Human skeletal muscle-derived CD133(+) cells form functional satellite cells after intramuscular transplantation in immunodeficient host mice. Mol Ther 2014;22:1008–17.

52. Miller RG, Sharma KR, Pavlath GK, et al. Myoblast implantation in Duchenne muscular dystrophy: the San Francisco study. Muscle Nerve 1997;20:469–78.

53. Partridge T. Myoblast transplantation. Neuromuscul Disord 2002;12:S3–6.

54. Premer C, Blum A, Bellio MA, et al. Allogeneic mesenchymal stem cells restore endothelial function in heart failure by stimulating endothelial progenitor cells. EBioMedicine 2015;2:467–75.

55. Baraniak PR, McDevitt TC. Stem cell paracrine actions and tissue regeneration. Regen Med 2010;5:121–43.

56. Murphy MB, Moncivais K, Caplan AI. Mesenchymal stem cells: environmentally responsive therapeutics for regenerative medicine. Exp Mol Med 2013;45:e54.

57. Taguchi A, Soma T, Tanaka H, et al. Administration of CD34+ cells after stroke enhances neurogenesis via angiogenesis in a mouse model. J Clin Invest 2004;114:330–8.

58. Bird TG, Lu WY, Boulter L, et al. Bone marrow injection stimulates hepatic ductular reactions in the absence of injury via macrophage-mediated TWEAK signaling. Proc Natl Acad Sci U S A 2013;110:6542–7.

59. Chimenti I, Smith RR, Li TS, et al. Relative roles of direct regeneration versus paracrine effects of human cardiosphere-derived cells transplanted into infarcted mice. Circ Res 2010;106:971–80.

60. Tang J, Wang J, Guo L, et al. Mesenchymal stem cells modified with stromal cell-derived factor 1 alpha improve cardiac remodeling via paracrine activation of hepatocyte growth factor in a rat model of myocardial infarction. Mol Cells 2010;29:9–19.

61. Bareja A, Billin AN. Satellite cell therapy: from mice to men. Skelet Muscle 2013;3:2.

62. Järvinen TA, Järvinen TL, Kääriäinen M, Kalimo H, Järvinen M. Muscle injuries: biology and treatment. Am J Sports Med 2005;33:745–64.

63. Scholz D, Thomas S, Sass S, Podzuweit T. Angiogenesis and myogenesis as two facets of inflammatory post-ischemic tissue regeneration. Mol Cell Biochem 2003;246:57–67.

64. Frey SP, Jansen H, Raschke MJ, Meffert RH, Ochman S. VEGF improves skeletal muscle regeneration after acute trauma and reconstruction of the limb in a rabbit model. Clin Orthop Relat Res 2012;470:3607–14.

65. Lepper C, Partridge TA, Fan CM. An absolute requirement for Pax7-positive satellite cells in acute injury-induced skeletal muscle regeneration. Development 2011;138:3639–46.

66. Negroni E. In vivo myogenic potential of human CD133+ muscle-derived stem cells: a quantitative study. Mol Ther 2009;17:1771–8.

67. Ehrhardt J, Brimah K, Adkin C, Partridge T, Morgan J. Human muscle precursor cells give rise to functional satellite cells in vivo. Neuromuscul Disord 2007;17:631–8.

68. Dellavalle A, Sampaolesi M, Tonlorenzi R, et al. Pericytes of human skeletal muscle are myogenic precursors distinct from satellite cells. Nat Cell Biol 2007;9:255–67.

69. Dezawa M, Ishikawa H, Itokazu Y, et al. Bone marrow stromal cells generate muscle cells and repair muscle degeneration. Science 2005;309:314–7.

70. Pesce M, Orlandi A, Iachininoto MG, et al. Myoendothelial differentiation of human umbilical cord blood-derived stem cells in ischemic limb tissues. Circ Res 2003;93:e51–62.

71. Pisciotta A, Riccio M, Carnevale G, et al. Stem cells isolated from human dental pulp and amniotic fluid improve skeletal muscle histopathology in mdx/SCID mice. Stem Cell Res Ther 2015;6:156.

72. Pinheiro CH, de Queiroz JC, Guimarães-Ferreira L, et al. Local injections of adipose-derived mesenchymal stem cells modulate inflammation and increase angiogenesis ameliorating the dystrophic phenotype in dystrophin-deficient skeletal muscle. Stem Cell Rev 2012;8:363–74.

73. Lavine L, Upcott H. Myocardial ischaemia treated by graft of skeletal muscle to the heart. Proc R Soc Med 1937;30:772.

74. Ebelt H, Jungblut M, Zhang Y, et al. Cellular cardiomyoplasty: improvement of left ventricular function correlates with the release of cardioactive cytokines. Stem Cells 2007;25:236–44.

75. Tang YL. Cellular therapy with autologous skeletal myoblasts for ischemic heart disease and heart failure. Methods Mol Med 2005;112:193–204.

76. Menasché P, Hagège AA, Scorsin M, et al. Myoblast transplantation for heart failure. Lancet 2001;357:279–80.

77. Vono R, Fuoco C, Testa S, et al. Activation of the pro-oxidant PKCβII-p66Shc signaling pathway contributes to pericyte dysfunction in skeletal muscles of patients with diabetes with critical limb ischemia. Diabetes 2016;65:3691–704.

KEY WORDS allogeneic progenitor cells, growth factors, PICs, porcine preclinical model, regeneration, skeletal muscle

APPENDIX For supplemental figures and table, please see the online version of this paper.